COXSACKIEVIRUS ADENOVIRUS RECEPTOR LOSS IMPAIRS ADULT NEUROGENESIS, SYNAPSE CONTENT and HIPPOCAMPUS PLASTICITY

Charleine Zussy[1,2]*, Fabien Loustalot[1,2]*, Felix Junyent[1,2]*, Fabrizio Gardoni[3], Cyril Bories[4], Jorge Valero[10], Michel G Desarménien[2,5], Florence Bernex[6], Daniel Henaff,[1,2], Neus Bayo-Puxan[1,2], Jin-Wen Chen[7], Nicolas Lonjon[8], Yves de Koninck[4], João O. Malva[10], Jeffrey M Bergelson[7], Monica di Luca[3], Giampietro Schiavo[9], Sara Salinas[1,2#] and Eric J Kremer[1,2#]

[1]Institut de Génétique Moléculaire de Montpellier, Montpellier, France
[2]Université de Montpellier, Montpellier, France
[3]Università degli Studi di Milano, Department of Pharmacological Sciences & Centre of Excellence on Neurodegenerative Diseases, Milan, Italy
[4]Mental Health Institute of Quebec, Quebec City, QC, Canada, and Department of Psychiatry and Neuroscience, Faculty of Medicine, Laval University, Quebec City, QC, Canada
[5]Institut de Génomique Fonctionnelle, CNRS, Inserm, Montpellier, France
[6]Institut Régional du Cancer Montpellier, Inserm, Montpellier, France
[7]Division of Infectious Diseases, Children's Hospital of Philadelphia, Philadelphia, PA, USA
[8]Département de Neurochirurgie, Hôpital Gui de Chauliac, Montpellier, France
[9]Sobell Department of Motor Neuroscience and Movement Disorders, UCL Institute of Neurology, Queen Square, London, United Kingdom
[10]Center for Neuroscience and Cell Biology, Faculty of Medicine, University of Coimbra, Coimbra, Portugal

*These authors contributed equally
[#]Correspondence to: sara.salinas@inserm.fr or eric.kremer@igmm.cnrs.fr

Abstract

While we are beginning to understand the late stage of neurodegenerative diseases, the molecular defects associated with the initiation of impaired cognition are poorly characterized. Here, we demonstrate that in the healthy adult brain, the cell adhesion molecule coxsackievirus and adenovirus receptor (CAR) is preferentially expressed on immature neurons in the hippocampus and enriched at the pre-synapse in some mature neurons. In a diseased or pro-inflammatory environment, CAR is lost from immature neurons in the hippocampus. Strikingly, in hippocampi of humans at early stages of late-onset Alzheimer's disease (AD) CAR is significantly reduced. Similarly, in triple-transgenic AD mice hippocampi, CAR levels are low and further reduced following systemic inflammation. Genetic deletion of CAR from the mouse brain triggers deficits in adult neurogenesis and synapse homeostasis that leads to impaired hippocampal plasticity and cognitive deficits. We propose that CAR loss of function contributes to cognitive defects in healthy and diseased-primed brains.

Introduction

Cell adhesion molecules (CAMs) are multifunctional proteins that play various roles in all tissues in cell-cell, cell-extracellular matrix attachment, migration, signalling and ion transport[1]. CAMs like the cadherins, ephrins, neurexins, and NCAM, a member of the Ig superfamily, play critical roles in general brain homeostasis[2]. CAMs regulate adult neurogenesis, dendritic spine development, and synapse remodelling - which combined form the bases of neuronal plasticity. During synaptogenesis, CAMs influence axonal growth, path finding and target recognition, the differentiation of pre- and post-synaptic specializations, and the regulation of synapse size, stability, strength and plasticity[3]. When defects in CAM functions occur, it invariably leads to neurological and psychiatric diseases[2]. In combination with genetic triggers, a compounding and unifying factor in the physiopathology of many brain diseases is a pro-inflammatory environment[4] that perturbs synapse homeostasis and adult neurogenesis. A pro-inflammatory environment, whether initiated in the brain or systemically, is responsible for impaired cognition in the healthy brain and amplifies cognitive defects in many neurodegenerative diseases, including Alzheimer's disease (AD)[5-7]. Pro-inflammatory cytokine-induced cognitive defects can be recapitulated in healthy mice and AD mouse models[8-10], highlighting the global repercussions of pro-inflammatory cytokines and chemokines in brain homeostasis. Conspicuously, the mechanistic link is poorly understood.

The coxsackievirus and adenovirus receptor (CAR) is a single-pass transmembrane protein belonging to the CTX subfamily of the immunoglobulin (Ig) superfamily[11]. Its extracellular region contains two globular Ig-like domains and a cytoplasmic tail that harbours protein interacting motifs. CAR functions are best characterized in epithelial cells, where it acts as a CAM and participates in the maintenance of tight junctions[12]. As the name suggests, CAR was identified as an attachment molecule for group B coxsackieviruses and some adenoviruses[13], including canine adenovirus type 2 (CAV-2)[14]. Because CAV-2 vectors have the ability to preferentially infect neurons and can be efficiently transported from axon terminals to efferent regions[15-23], the vectors have become powerful tools to investigate

anatomical organization of neural circuits and higher-order brain functions, and to treat brain diseases. Existing data indicate that CAR is responsible for CAV-2 neuron binding, entry, retrograde axonal transport and preferential gene transfer after intraparenchymal injections[14,24,25]. In addition, CAV-2 engagement of CAR may cause its transient depletion[65] and affect downstream biological assays CAR.

Although a role for CAR in brain development has been proposed[26,27], its cellular and subcellular location, and functions in the adult brain are poorly characterized. Here, we demonstrate that in the healthy brain CAR is abundant in axon tracks throughout the brain, on the soma of neuroprecursor cells (NPCs), in the mossy fibres of the stratum lucidum, at the pre-synapse in some mature neurons, and recruited to activated pre-synapses. Genetic deletion of CAR perturbs adult neurogenesis, synaptic homeostasis, and behaviour in mice. In addition, we show that a pro-inflammatory environment induced by AD and/or systemic inflammation causes CAR loss in the hippocampus. Together, our data link posttranslational CAR loss in the hippocampus to inflammation, modulation of hippocampal plasticity, and impaired cognition in healthy and diseased brain.

Results

CAR is enriched in axons, at the presynapse, and on the soma of cells in the DG

Following CAV-2 vector injection into the mammalian brain parenchyma, transgene expression is predominantly in neurons[28,29]. As CAR appears to be the exclusive attachment molecule for CAV-2 vectors *in vitro*, we previously proposed that CAR expression is likely restricted to neurons[24,30]. To characterize CAR cellular and subcellular location we analysed the distribution of CAR in the brain of 2-month-old mice by immunohistochemistry (IHC) and immunofluorescence (IF). CAR staining is notable in the posterior corpus callosum, between layers IV and V of the cerebral cortex, and in layer I of the cerebral cortex, which is primarily axons from other cortical areas and apical dendrites of local neurons (Fig 1A). In the hippocampus CAR staining is in the axons projecting from the entorhinal cortex, as well as in mossy fibres in the stratum lucidum (SLu) (Fig. 1B & C). Despite strong axon labelling in most regions, the cell bodies of mature neurons are strikingly devoid of CAR. However, somatic CAR staining was notable in some cells the subgranular zone (SGZ) and their projections in the granular cell layer (GCL) of the dentate gyrus (Fig 1B & D). In contrast to a previous report[31], we do not detect CAR in cells with glia-like morphology.

In addition to the preferential transduction of neurons, CAV-2 vector transport from the injections site to cell bodies in efferent regions is remarkably efficient in some neuron types, suggesting that CAR is likely located along axon projections[15-21,28]. To address CAR subcellular distribution in neurons, we isolated and separated synaptosomes[32] from 2-month-old mouse brains. Similarly to other synaptic proteins, CAR is enriched in the synaptosome fraction (Fig. 1E). In epithelial cells, CAR forms high affinity intercellular homodimers via its globular D1 and D2 Ig-like domains. To determine if this intercellular homodimeric interaction is similar at the highly specialized neuron synapse, we separated the post-synaptic density (PSD) from the pre-synaptic compartment. While the biochemical separation of these two fractions is not without minor cross-contamination, we nonetheless find CAR enriched in the

pre-synapse fraction, and absent in the PSD (Fig. 1E). CAR is also preferentially located at the presynapse in the human brain (Supplementary Fig 1A).

To address CAR location using another approach, we stained mature (> DIV14) primary hippocampal neurons for CAR. In mature neurons, CAR is present in the somato-dendritic and axonal compartments and colocalized with the synaptic marker synaptophysin (Fig. 1F). In addition, CAR puncta overlap with VGLUT, VGAT and PSD95 (Supplementary Fig. 1B), demonstrating that using, these culture conditions, CAR is present at the synapse in excitatory and inhibitory synapses. Consistent with the biochemical assays, at DIV 21, when dendritic spines are fully mature, we are unable to detect CAR in dendritic spines, consistent with the lack of CAR at or near the post-synapse (Fig. 1G).

Together, these data demonstrate that CAR is preferentially expressed by neurons in the mouse brain, on the soma of cells in the SGZ of the DG and their axons projecting to the CA3 (mossy fibres in the stratum lucidum), and axons projecting from the entorhinal cortex. CAR is also enriched at the pre-synapse, where CAR-CAR interactions are not occurring in *trans*.

CAR loss of function impacts hippocampal granular cell layer organisation

To better understand CAR function(s) in the brain we generated conditional CAR CNS KO (CAR-CNS^{KO}) mice by crossing nestin-Cre[33] and CAR$^{flox/flox}$ mice[34] (Supplementary Fig. 2A). CAR-CNS^{KO} mice thrived, have no detectable CAR expression in the brain by western blot assays (Fig. 2A) or when assaying by IHC (Supplementary Fig. 2B). These IHC analyses in CAR-CNS^{KO} mice confirm the specificity of the CAR antibodies and staining in control mice (Fig 1A). The CAR-CNS^{KO} mice have no obvious phenotypic differences compared to WT mice. Macroscopic histology using cresyl violet staining of 2-month-old wild type (WT), CAR$^{flox/flox}$ (hereafter referred to as control), and CAR-CNS^{KO} mice suggested that there are no gross morphological anomalies in the CAR-CNS^{KO} mouse brain (Supplemental Fig. 2C). However, upon detailed examination we found that the granular cell layer (GCL) of the DG in CAR-CNS^{KO} mice is less densely packed and occupies a significantly greater area than in

control littermates (Fig. 2B & C). This difference in area is significant for the GCL, but not for the pyramidal layer of CA1 or CA3 (Supplementary Fig. 2D).

These data suggest that CAR loss of function may affect new neuron integration in the GCL.

Impaired adult hippocampal neurogenesis in CAR-CNS^{KO} mice

Adult neurogenesis influences learning and memory by the generation and integration of new neurons into existing networks[35]. In the adult mouse brain, neurogenesis is thought to be restricted to the subventricular zone (SVZ) and in the SGZ of the DG in the hippocampus[36]. As there was a notable defect in the organization of the GCL of the DG, and CAR is readily detected on the cell body of a subpopulation of cells in the SGZ, we co-incubated sections with anti-CAR and anti-PSA-NCAM antibodies (PSA-NCAM is a marker of immature neurons). We found that the majority of cells expressing CAR on the cell body and axons in the inner layer of the DG are PSA-NCAM^{+} neurons (Fig. 2D & E). Costaining with CAR and NeuN (marker of mature neurons) show that some “NeuN-low” cells also have CAR staining on the cell body (Fig. 2F). To determine if CAR is expressed by adult NPCs using another approach, we generated neurospheres from NPCs isolated from the SGZ of the adult mouse brain. Neurospheres in suspension and those induced to attach to polyornithine-coated glass slides are also CAR^{+} (Supplementary Fig. 3A).

We then asked whether CAR loss of function affects proliferation, survival and/or differentiation of newborn neurons in the DG. To address this question proliferating cells in the brain of CAR-CNS^{KO} mice were labelled using thymidine analogues that incorporate into the genome of dividing cells. The fate of newborn CAR-negative cells in the DG was evaluated by comparing EdU^{+} cells in CAR-CNS^{KO} versus control mice. Mice sacrificed 1 day post-injection allow one to determine proliferation, while sacrificing mice at 28 days post-injection reflects neuron survival/differentiation. In both groups the number of EdU^{+} cells in the DG is similar (Fig. 2G & H). However there are significantly fewer EdU^{+} neurons (NeuN^{+}) in CAR-CNS^{KO} mice compared to control mice 28 days post-injection (Fig. 2I & Supplementary Fig 3B). The decrease in mature neurons is mirrored by an increase in the

164 percentage of EdU^+ immature ($PSA\text{-}NCAM^+$) neurons (Fig. 1J & Supplementary Fig 3C).
165 Because sex-related factors can differentially affect the brain, we assayed male and female
166 samples individually. However, in these assays, we did not detect sex differences. Together,
167 these data demonstrate that adult NPC proliferation and survival are not affected, but
168 differentiation is, demonstrating a role for CAR in adult neurogenesis.

169 **Synapses are perturbed in the CAR-CNS^{KO} mouse hippocampus**

170 Because CAMs can also be targeted to synapses during plasticity[37], we asked if activation or
171 chemical-induction of long-term potentiation (LTP) affects presynaptic CAR**.** We therefore
172 compared the location of synaptophysin and CAR after neuronal depolarisation[38]. We found
173 by measuring CAR/synaptophysin colocalisation that percentage of CAR^+ synapses increase
174 (Fig. 3A & Supplementary Fig. 4B). We then asked if CAR levels change at the synapse
175 following induction of neuronal plasticity. To this end, we incubated hippocampal neurons
176 with BDNF[39] and quantified of CAR/synaptophysin colocalisation. Using this assay we found
177 that CAR can be recruited to synaptic termini (Fig. 3B).

178 Synaptic plasticity also involves a feedback loop to ensure the production and targeting of
179 actors involved in neurotransmission through recruitment/exclusion of proteins, local mRNA
180 translation, and transcription. We then asked if CAR loss of function affects synapse content
181 and/or genesis. To monitor synaptic protein content in the hippocampus of CAR-CNS^{KO} mice,
182 the levels of several *bona fide* synapse proteins were quantified by immunoblotting. In male
183 CAR-CNS^{KO} mice VGAT and synaptophysin are significantly decreased compared to controls
184 (Fig. 3C). Unexpectedly, in CAR-CNS^{KO} female mice most synapse protein levels are lower
185 compared to female control mice (Fig. 3D).

186 Together, these data demonstrate that CAR modulates synaptic function in a sex-biased
187 manner through its direct recruitment and/or by influencing synaptic protein levels.

188 **CAR loss perturbs hippocampal synaptic plasticity**

Because CAR loss of function affects the organization of the DG, adult neurogenesis and global hippocampal synapse content, we asked whether the general plasticity of hippocampal neurotransmission is affected. We therefore measured short-term plasticity as paired-pulse facilitation (PPF, measured as paired-pulse ratio; PPR) and long-term plasticity as LTP induction and maintenance in organotypic slices from CAR-CNS^{KO} mice. Schaffer collaterals were stimulated and evoked field extracellular excitatory postsynaptic potentials (fEPSPs) were recorded in the stratum radiatum of the CA1 area (Supplementary Fig. 4A). After 10 min of stable recording baseline activity, high-frequency stimulations (HFS) were applied to induce LTP (Fig. 4A). No significant differences are observed between PPRs from male CAR-CNS^{KO} and control males, before or 60 min post-HFS (Fig. 4B). By contrast, PPRs from CAR-CNS^{KO} females are significantly lower than PPRs from control females (Fig. 4C). To visualize LTP, the level of post-HFS potentiation is expressed as a percentage of the mean fEPSP amplitude before LTP induction. CAR-CNS^{KO} and control males have comparable level of LTP as observed by the increased fEPSPs peaks post-HSF for both groups (Fig. 4D). Conversely, CAR-CNS^{KO} females present significant deficits compared to control females (Fig. 4E), as the levels of post-HFS potentiation in CAR-CNS^{KO} females rapidly decrease. After 60 min, the amplitude of the fEPSPs in CAR-CNS^{KO} females is not different from baseline activity, while in control females increased fEPSPs peaks are observed from 10 to 60 min post-HSF.

Together, these data demonstrate that CAR loss of function perturbs synaptic plasticity in the hippocampus in a sex-biased manner. We concluded that loss of function of pre-synaptic CAR affects neurotransmission in the hippocampus.

CAR loss of function impacts behaviour

Adult neurogenesis and synapse homeostasis are processes associated with cognition. We therefore subjected CAR-CNS^{KO} mice to a series of behavioural tests that are associated with hippocampal functions. Because CAR is expressed at the neuromuscular junction (see references[15,28]) and locomotion and exploration deficits can interfere with cognitive tasks, we

initially examined the mobility of mice in an open-field paradigm. Neither the distance travelled, nor locomotion speed, is significantly different between control and CAR-CNS^{KO} mice (Supplementary Fig. 5). By contrast, in the elevated plus maze, male and female CAR-CNS^{KO} mice spend less time in the open arm compared to control mice, reflecting an abnormal level of anxiety (Fig. 5A). In the Y maze, a nonaversive task based on rodents' natural exploratory instincts, spontaneous alternation performances are impaired in male and female CAR-CNS^{KO} mice (Fig. 5B), reflecting a spatial working memory deficit. In Morris water maze tasks, male and female CAR-CNS^{KO} mice show a higher latency to find the hidden platform in the training quadrant compared to control littermates on days 2-5 (Fig. 5C), demonstrating an altered learning process. In the probe trial conducted 24 h post-training, both control and CAR-CNS^{KO} male mice swim preferentially in the training quadrant during the 60 s session (Fig. 5D). By contrast, the time spent in the training quadrant is near the random values for female CAR-CNS^{KO} mice (Fig. 5E), demonstrating that the retention of spatial memory is altered in female CAR-CNS^{KO} mice.

Together, our data demonstrate a role for CAR in hippocampal plasticity in a sex-biased manner and underscore a function in cognitive processes such as spatial memory.

Decreased CAR levels in the pro-inflammatory environment of the AD brain

To the best of our knowledge, mutations in the CAR gene (*CXADR*) are not linked with brain dysfunction. This is likely because CAR plays primordial roles in other tissue like the heart, where loss of function is embryonically lethal[34]. However, there are posttranscriptional mechanisms that can lead to the loss of CAR: studies using non-neuronal cells and tissues suggested that CAR levels are indirectly reduced by pro-inflammatory cytokines (*e.g.* TNF-α and INF-γ)[40,41]. In addition, CAR is a substrate for α, β and γ-secretases implicated in the pathogenesis of AD[42,43]. These observations led us to assay CAR levels in primary murine hippocampal neurons after ionomycin-induced secretase activation and TNF-α and INF-γ treatment. As a positive control for CAR loss we incubated hippocampal neurons with the CAV-2 fibre knob (FK^{CAV}) (Fig. 6), which disrupts homodimeric CAR interactions and induces

CAR internalization and lysosomal degradation in neuronal cells[62]. Following ionomycin treatment, the levels of the CAR ectodomain increase in the cell culture supernatant and full-length CAR decreases in total cell extract (Fig. 6A). CAR levels also significantly decrease in primary cultures of murine hippocampal neurons and adult murine NPCs incubated with TNF-α and INF-γ in a dose-dependent response (Fig. 6B-D). CAR levels also decrease in human NPCs derived from IPS cells (Supplementary Fig. 6).

Systemic inflammation perturbs brain function via several overlapping mechanisms, including pro-inflammatory cytokines entering in the brain after systemic inflammation or via microglia activation and cytokine secretion in the brain[10]. We therefore asked if global CAR levels in the brain are affected by systemic inflammation. To address this possibility we injected lipopolysaccharides (LPS) into the peritoneal cavity of healthy mice and quantified CAR levels by immunoblotting. At 1 or 7 weeks postinjection we do not detect a significant change in global CAR levels as assayed by immunoblotting in any region, including the hippocampus (Supplementary Fig. 7). In contrast to the diffuse CAR staining throughout the axon tracks in most of the brain, (Fig 1A) NPCs have high levels of somal CAR. We therefore asked if the somal CAR population is affected by systemic LPS injection. At 1 week post-LPS injection, CAR staining is strikingly reduced in immature neurons in the DG, and their axons that project to CA3 while PSA-NCAM staining is unaffected (Fig. 6E). These data suggest that during acute induction of pro-inflammatory cytokines by systemic stimuli somal CAR levels on NPC are affected. This difference in susceptibility to a pro-inflammatory environment suggests different CAR binding partners and/or function during neurogenesis.

Activated secretases[44] and a pro-inflammatory environment[45] are closely linked hallmarks of several neurodegenerative diseases and create a feed-forward loop. In AD, an inflammatory environment can lead to increased β-secretase (BACE1: β-site amyloid precursor protein (APP)-cleaving enzyme) expression, Aβ overproduction, and senile plaque accumulation[46] – which in turn promote an NF-κB pro-inflammatory cytokine response. Because inflammation, synapse homeostasis and perturbation of CAM functions can be associated with neurologic

and psychiatric diseases[47-49] – in particular late-onset AD, which is inexorably linked with inflammation – we asked if CAR levels are perturbed in the AD hipoccampus. 3xTgAD mice recapitulate some AD-related characteristics such as increased level of pro-inflammatory cytokines, age-related formation of senile plaques, neurofibrillary tangles, impaired synapse homeostasis and cognitive functions[50-52]. Therefore, we compared CAR levels in total protein extracts from hippocampi from age-matched controls and 5 to 8-month-old (transitional stage of AD progression) and 16 to 20-month-old (late stage of AD progression) 3xTgAD mice. CAR is significantly reduced in both 3xTgAD mouse age groups, with a greater decrease in the older cohort compared to age-matched controls (Fig. 7A & B). To determine if the decrease is due to a pre- or post-translation mechanism, we quantified *Cxadr* (the murine CAR gene) mRNA levels using the same samples (Fig. 7C). We did not detect a difference of *Cxadr* mRNA levels between WT and 3xTgAD animals in either group consistent with post-translational CAR loss.

We (*JV, JOM reference 8) previously showed that systemic inflammation induced by LPS injections impairs long-term spatial memory and neurogenesis in healthy and 3xTgAD mice[8]. LPS-induced defect in spatial memory is exacerbated in 3xTgAD mice and associated with a significantly reduction in the production the number of synaptic puncta[8]. We therefore asked whether systemic LPS-induced systemic inflammation exacerbated CAR loss in the 3xTgAD mouse brain. To address this possibility we injected LPS into the peritoneal cavity of control and 3xTgAD mice. Control and 3xTgAD mice with memory defects were sacrificed 7 weeks post-LPS injection and global CAR levels were quantified by immunoblotting. We found that global CAR levels (as assayed by immunoblotting) in LPS injected WT and 3xTgAD mice are not significantly different from PBS-injected controls (Supplementary Fig. 7). By contrast, IHC analyses show that CAR is strikingly absent from the soma and neurites of cells in the SGZ of the DG and in the mossy fibres of the stratum lucidum following LPS injections (Fig 7D). Quantification of CAR staining (Fig 7E) show that CAR staining is significantly lower in PBS-injected 3xTgAD mice versus control healthy mice. More noteworthy, LPS injections

297 significantly reduce the number of CAR^+ immature neurons in healthy and 3xTgAD mice
298 versus PBS-injected controls.

299 Together, these data demonstrate that CAR can be lost from the hippocampus in healthy and
300 AD mouse brains, likely via a posttranslational mechanism induced by systemic
301 inflammation. CAR loss in the adult mouse hippocampus is congruent with memory defects.

302 **CAR levels in the hippocampus of human AD patients**

303 Extrapolating results from mice to human neurodegenerative diseases has historically been
304 challenging. Therefore, we assayed protein extracts from hippocampi from Braak IV stage
305 AD patients and age-matched controls[53]. Braak staging is used to classify the degree of
306 pathology in post-mortem AD brains and Braak IV neurofibrillary tangle can be seen in the
307 limbic regions. In the hippocampus of these AD patients, the level of several synapse
308 proteins, including synaptophysin and SNAP25, are not altered[53] demonstrating that
309 significant synapse loss had not yet occurred. Remarkably though, CAR levels are
310 significantly decreased already at Braak IV stage of late-onset AD (Fig. 7F & G).

311 Together, these data demonstrate that CAR levels are significantly reduced in the human AD
312 brain when impaired cognition starts, but dementia is not yet declared.

313

Discussion

Prior to this study, there were no known roles for CAR in the adult brain. Here, we demonstrate that in the healthy adult brain CAR has cell type-specific functions. CAR is predominantly located on neuron projections and enriched at the pre-synapse, where it can be recruited upon stimulation. In the hippocampus, CAR staining is notable on the soma and projections of immature PSA-NCAM^{+} neurons in the GCL of the DG. In the CAR-CNS^{KO} mouse brain, CAR loss of function perturbs synapse content, LTP and adult neurogenesis, which together affect behaviour. When healthy mice are challenged with LPS-induced systemic inflammation, CAR levels notably decrease in the neurogenic niche of the DG. In the diseased-primed brain, we demonstrate that CAR levels are significantly decreased in the hippocampus of humans during the early phase of late-onset AD, and in 3xTgAD mice. CAR levels are further reduced in 3xTgAD mice challenged with LPS injected into the peritoneal cavity. Based on these combined results we propose a link between CAR loss of function and hippocampus-associated cognitive impairments such as those found in the early stages of late-onset AD. Clearly, the likely connections between CAR-linked defects in adult neurogenesis, synaptic plasticity and cognitive tasks, and the reduction of synaptic protein levels in the hippocampus, will require focused and extended analyses in each area.

CAR in the healthy brain

Neuronal plasticity arises from processes ranging from adult neurogenesis, dendritic spine development and synapse remodelling. In the hippocampus, we found overlapping pattern of expression/localisation between CAR and PSA-NCAM. The similarities between CAR and PSA-NCAM are notable: both are widely expressed in the embryonic and early postnatal brain. In the adult brain, PSA-NCAM is confined to restricted areas in the DG, where its expression corresponds to the period when post-mitotic neuroblasts extend their processes and migrate. Notably, CAR and PSA-NCAM are also readily detected in the mossy fibre in the stratum lucidum. After new neurons reach the granular cell layer and develop into mature granule cells, PSA-NCAM[55] and CAR expression are downregulated and restricted to specific

compartments. These immature neurons expressing CAR and PSA-NCAM have unique functional properties including enhanced synaptic plasticity and lower threshold for the induction of glutamatergic potentiation[56]. These properties make them susceptible to be recruited upon hippocampal activation[57]. While the concept of synaptic plasticity is usually associated with functional modifications in pre-existing synapses (like LTP), it includes structural changes as well, including formation and elimination of synapses. In primary cultures of hippocampal neurons, which resemble immature neurons in the adult hippocampus, CAR is recruited to the synapse. These observations underscore the potential role of CAR in neuronal circuit remodelling regulating hippocampal plasticity. It will be primordial to determine whether hippocampal CAR, like NCAM, is modulated pre- or post-translationally following behavioural tasks[58,59], contextual fear conditioning[60] or passive avoidance[61].

In the adult brain, NCAM stabilizes neural circuits, while the polysialylation of NCAM induces anti-adhesion properties, allowing structural plasticity of neuronal network, including activity-dependent synaptic plasticity and formation of long-term memory[62-64]. In epithelial cells, abolishing glycosylation of the extracellular domains of CAR can reduce intercellular adhesion[65]. How this occurs is unclear. Could glycosylation limit intracellular *cis* CAR-CAR interactions[27] and influence CAR function in NPCs or in neurons? In some adult neurons CAR, like non-polysialylated NCAM, may enable interactions that induce neuronal and neurite outgrowth[27,66]. Although our data in the brain of CAR-CNS^{KO} mice poorly dovetail with a primordial role for CAR during axon guidance[24], we cannot exclude the possibility that CAR plays a role in axon guidance in a subset of neurons.

Assuming that CAR will behave, at least in some respects, as a prototypical CAM with the noncanonical functions[1] it would not be surprising that once recruited to synapses CAR interacts with a different intracellular and extracellular partners than those in the soma. Among synaptic CAMs, integrins play a role in LTP by controlling actin reorganisation and spine remodelling in an NMDA-dependent mechanism[67]. Notably, fibronectin, the

368 extracellular matrix protein mediating integrin effects, also binds CAR to promote neurite
369 extension *in vitro*[27].

370 **Losing CAR and affecting neurogenesis**

371 Both intrinsic and extrinsic mechanisms regulate adult neurogenesis. Like some NCAM
372 isoforms[68], our data are consistent with a role for CAR in NPC differentiation and integration
373 in existing circuitries. Based on the IHC staining, the majority of CAR in the brain is in axon
374 tracks - and the majority of CAR in the brain is not lost following acute LPS-induced
375 inflammation in mice. A striking exception is CAR on the cell body of immature neurons.
376 CAM processing by secretases regulates neuron proliferation, migration and plasticity. The
377 juxtaposition of these observations begs the question of whether CAR processing on
378 immature neurons is a fundamental event during neurogenesis. In addition to BACE1, CAR
379 is also a substrate for α and γ-secretases, which can liberate CAR ectodomain and
380 intracellular domain[42]. Protease cleavage of CAR could switch its role to signalling molecules
381 by the generation of intracellular domains[69]. A phosphorylated fragment of the CAR
382 intracellular domain can be found in the nucleus[70], and therefore may influence
383 transcriptional regulation, which could impact neurogenesis and/or synapse homeostasis.

384 Adult human neurogenesis creates around 700 neurons/day in the DG[71], which over an
385 average life span corresponds to approximately one third of the total numbers of neurons in
386 the entire hippocampus (or to the equivalent of the renewal of the DG). In CAR-CNS^{KO} mice
387 the disorganization of the GCL in the DG is consistent with abnormal neuron integration. A
388 similar phenotype is found in mice lacking Reelin, which modulates CAM-dependent
389 migration[72], and therefore CAR loss of function may impair similar guidance cues.

390 **CAR, hippocampal plasticity and AD**

391 As the decade-long progression to AD symptoms occurs, synapse function and adult
392 neurogenesis are battered by recurring acute and/or chronic pro-inflammatory insults.
393 Similarly to the AD brain[36], adult neurogenesis and synapse function are perturbed in CAR-

CNS^{KO} mice. In 3xTgAD mice, a decrease in adult NPC proliferation correlates with the presence of senile plaques and of Aβ-containing neurons[73]. These stimuli increase the TNF-α and INF-γ production, which can directly increase γ-secretase activity through a JNK-dependent MAPK pathway[54]. As CAR is also processed by α, β and γ-secretase[42,43] the link between systemic LPS injections and CAR loss in the hippocampus is coherent, but will need further analyses.

CAR at the synapse

In some murine models of brain disorders, synapse content is altered in an age-dependent process and parallels the onset of cognitive deficits[50,74]. Many components of AD pathophysiology affect neurogenesis and synapse homeostasis and the onset of impaired cognition in AD is an enigma: histological analyses of brains from suspected early stage AD patients have no striking differences compared to age-matched controls. Yet, synapse dysfunction occurs early in AD, followed by a gradual pre-synapse and spine loss that occurs over decades[5]. Notably, at Braak IV, severe synapse loss has not occurred yet. It was surprising to previously find that after acute CAR depletion in the 6-week old mouse striatum, a return to pre-depletion levels takes at least one month[75]. It would not be unexpected to find that CAR replacement is significantly slower in the aged human brain, and therefore repeated acute CAR depletion would have a cascading effect on hippocampal plasticity. Our data demonstrating that CAR levels are significantly reduced at early stages of late-onset AD, and before most synaptic protein levels are changed, underscore CAR's role in hippocampal plasticity and its likely impact in AD-related cognitive impairment.

CAR and the sexes

Decades of studies trying to identify a mechanistic reason why women are more susceptible to AD[76] have not led to a consensus[77]. Conspicuously, female CAR-CNS^{KO} mice are more affected in synapse content, short- and long-term synaptic plasticity and in memory retention. One plausible explanation for sex-biased difference is sex steroid concentrations, as the hippocampus synthesises estrogen and androgen. Estradiol levels in the hippocampus are 8

nM in male rodents, but only 0.5 – 2 nM in females[78]. Numerous studies show that estrogens have neuroprotective properties and improve plasticity and memory processes[79]. It is conceivable that in male mice higher levels of steroids mask the more severe impairment observed in female CAR-CNS^{KO} mice. As noted previously, translational studies from rodents to humans, especially for neurodegenerative diseases, are challenging to interpret. We are tempted to speculate that in humans there is a link between estrogen and the *CXADR* promoter, as it possesses an estrogen-responsive element[80]. More efficient replacement of inflammation-induced depleted CAR in the male brain - via estrogen-induced transcription - would fit attractively into the existing data.

In conclusion, we characterize CAR expression in the healthy and diseased brain and show that it is a multifunctional protein in immature and some mature neurons. Using transgenic mice depleted in CAR expression in the brain we identify roles for CAR during adult neurogenesis and in synapse biology. In the healthy and diseased brain, we delineate a pathway where secretases and pro-inflammatory cytokine insults perturb CAR levels and affect adult neurogenesis, synapse homeostasis and hippocampal plasticity. We propose that the consequence of recurrent or chronic pro-inflammatory insults combined with the etiological origin of the neurodegenerative diseases, impact CAR function and ultimately reaches a threshold in aged and diseased brain and exacerbate cognitive decline.

Material and Methods

Ethics

Mice were treated in accordance with the European Community Council Directive 86/609, modified by the decrees 87/848 and 2001/464. The Animal Welfare Committee at the University of Montpellier II approved all protocols and all efforts were made to minimize the number of animals used and potential pain and distress. Human brain samples were processed in accordance with European bioethics laws regarding patient information: written consent was obtained from participant. Human tissue was obtained from the approach in a non-pathological area for resection of temporal low-grade tumour. AD and control hippocampal extracts have been previously described[53].

Mouse breeding and tissue samples

The generation of nestin-Cre mice and $CAR^{flox/flox}$ mice has been described[33, 34]. $CAR\text{-}CNS^{KO}$ mice were obtained by crossing these two strains. Mice were backcrossed during six generations on a C57BL/6J background. Animals were housed in groups, and allowed food and water *ad libitum*. They were maintained in a controlled environment (22 ± 1°C, 55 ± 5% humidity) with a 12 h: 12 h light/dark cycle. Unless specified otherwise, all experiments were performed on 2-month-old $CAR^{flox/flox}$ and $CAR^{flox/flox}$ nestin-Cre littermates. Genotyping was performed according to previously published methods[34]. 3xTgAD mice were described previously[51]. Animals used in histological procedures were anaesthetized with intraperitoneal injection of ketamine (100 mg/kg) and xylazine (10 mg/kg) and then perfused with 4% paraformaldehyde in 0.1 M phosphate buffer (PFA-PB). Brains were removed and post-fixed in PFA-PBS for 24 h, and then cryopreserved in a 30% sucrose solution. Fixed brains were frozen and cut in 40-µm-thick serial coronal sections with a cryostat.

Cresyl violet staining

Mice were terminally anesthetized using ketamine and xylazine before their intracardiac perfusion with 4% PFA. Brains were fixed overnight in 4% PFA and then embedded in

paraffin. Six animals in each group and 6 sections from each individual were used for quantification. Coronal slices (10-µm thick) were cut from each animal. Sections were stained with 0.1% cresyl violet and luxol fast blue reagents, dehydrated, and mounted. Slices were scanned with a Nanozoomer and captured with NDP view software (Hamamatsu). Quantitative histological measurements of the DG, CA1 and CA3 cell layers (granular and pyramidal respectively) were performed with NDP view software.

qRT-PCR

Total RNA was extracted from brain tissue (3xTgAD mice) using the RNeasy Mini kit (Qiagen) and reverse transcribed by using random hexamers primers (Roche) and SuprScript III Reverse Transcriptase (Invitrogen), according to the manufacturer's protocols. For quantitative analyses, primers that selectively amplify murine CAR were used (forward: TCTTCTGCTGTCACAGGAAAC and reverse: CTGGGGACTTGGTTATACTGC) and real-time PCR was performed using SYBR Green PCR mix and Light-Cycler 480 machine.

Primary hippocampal cultures and treatments

Primary hippocampal neurons were prepared from OF1 E18 mice embryos (Charles River) as previously described[75]. To study CAR involvement in neurotransmission, we used chemical protocols to induce depolarisation or LTP on mature hippocampal neurons (DIV21)[38,39]. Depolarisation was obtained by treating neurons with 90 mM KCl for 5 min (in 5 mM HEPES, 10 mM glucose, 2.5 mM $CaCl_2$, 1 mM $MgCl_2$, 137 mM NaCl). LTP was induced by treating neurons with 20 ng of recombinant BDNF (Peprotech) for 45 min. Assays with CAV-2 fibre knob (FK^{CAV}) were performed as previously described[75]. Murine TNF-α and INF-γ were purchased from PeproTech.

Immunohistochemistry and immunofluorescence studies

For CAR immunohistochemistry the following protocol was used: free-floating coronal sections of brain were rinsed in 0.1 M PB, pH 7.2, and then treated with 0.5 % H_2O_2 and 10% methanol in PBS for 15 min and washed with PBS. Sections were permeabilized with PBS-T

492 (PBS with 0.5% Triton X-100) and incubated for 1 h in blocking solution (10% FBS in PBS-T).
493 Afterwards, sections were incubated overnight at 4°C with goat anti-CAR (R&D). Sections
494 were then sequentially incubated for 2 h with biotinylated horse anti-goat antibody (Vector
495 Labs) and then incubated with the avidin-biotin-peroxidase complex (ABC, Vector Labs) prior
496 to peroxidase reaction. Stained sections were examined under the light microscope (Leica
497 DM6000).

498 For immunofluorescence, free-floating coronal sections of brain were rinsed in 0.1 M PB, pH
499 7.2, permeabilized with PBS-T and incubated for 1 h in blocking solution. Sections were then
500 incubated overnight at 4°C with goat anti-CAR (R&D) and with rabbit anti-sox2 (Abcam),
501 mouse anti-PSA-NCAM (Hybridoma bank) or mouse anti-NeuN (Millipore). Sections were
502 then sequentially incubated for 2 h with the corresponding AlexaFluor secondary antibodies
503 (Life Technology). Stained sections were examined using a Leica SP5 confocal microscope.

504 Dissociated primary neurons and murine NPCs were washed with PBS before their fixation
505 and permeabilization with PFA or with -20°C methanol/acetone. Cells were then washed
506 three times in PBS, and blocked for 30 min in PBS containing 2% BSA and 10% horse
507 serum. Cells were incubated with primary antibodies overnight at 4°C (a goat anti-CAR (R&D
508 system), a mouse anti-VGLUT, a rabbit anti-gephyrin, a mouse anti-VGAT (SYnaptic
509 SYstem), a mouse anti-PSD95 (Abcam), a mouse anti-synaptophysin (Sigma-Aldrich) and a
510 mouse anti-MAP2 (Roche), followed by three washes with PBS. Incubation with appropriate
511 AlexaFluor secondary antibodies was performed for 1 h at room temperature, followed by
512 three washes with PBS. The coverslips were mounted on slides with fluorescent mounting
513 media (DAKO) containing DAPI. Images were captured using a Zeiss LSM 780 confocal
514 microscope with ZEN imaging software.

515 **Analyses of synaptic proteins**

516 Presynaptic and postsynaptic protein from the hippocampus from 2-month-old control and
517 CAR-CNS^{KO} mice were assessed by western blotting. After behavioural studies, mice were
518 sacrificed by decapitation, and hippocampi were rapidly dissected, frozen and stored at -

519 80°C. Tissues were sonicated in 5% SDS and the protein concentration was measured using
520 the BCA Kit (Pierce, France). Five to fifteen µg of proteins were loaded, separated by SDS-
521 polyacrylamide gel (12%) and transferred to a PVDF membrane. Membranes were blocked
522 and incubated overnight (4°C) with a mouse anti-VGLUT, a mouse anti-VGAT, a rabbit anti-
523 gephyrin, a rabbit anti-GABA-A receptor gamma 2, a rat anti-NCAM 180 (SYnaptic SYstem),
524 a mouse anti-PSD95 (Abcam), a mouse anti-NR1 (Millipore), a mouse anti-synaptophysin
525 and a mouse anti-β-tubulin (β-tub) (Sigma-Aldrich). Membranes were then rinsed and
526 incubated for 1 h at room temperature with the appropriate horseradish peroxidase-
527 conjugated secondary antibodies (Sigma-Aldrich). Enhanced-chemiluminescence (ECL)
528 reagents were used to reveal peroxidase activity. The intensity of the bands was quantified
529 using Image-J software. Synaptic protein levels were normalized to β-tubulin levels.

530 **Murine NPCs and neurospheres cultures**

531 Mouse NPCs were isolated using a modified published protocol[81]. Six-weeks-old control and
532 CAR-CNS^{KO} females were used. SVZ was isolated by microdissection in HBSS 1X
533 supplemented with 30 mM glucose, 2 mM HEPES and 26 mM $NaHCO_3$. Cells dissociation
534 was carried out by enzymatic digestion using 0.0025% trypsin-EDTA (Life Technology)
535 during 5-10 min at 37°C. Complete dissociation has been accomplished by mechanical
536 dissociation using glass polished fire pipette. Cells were seeded in poly-ornithine (0.5 □g/mL
537 in PBS 1X, Sigma) and laminin (10 □g/mL in DMEM/F12, Sigma) coated dishes in
538 Neurobasal (Life Technology) supplemented with B27, GlutaMAX, penicillin/streptomycin, 20
539 ng/mL EGF and 20 ng/mL FGF_2 (PeproTech) at 37°C, 5% CO_2 and saturated humidity
540 atmosphere. Cell culture media was changed every 2 days until reaching 90% of confluence.
541 Cells were expanded and maintain in an undifferentiated state by seeding 10^5 cells/mL in
542 proliferating media DMEM/F12, N2, penicillin/streptomycin, 20 ng/mL EGF and 20 ng/mL
543 FGF_2 in polyornithine/laminin-coated dish.

544 Neurospheres were prepared from OF1 4 month-old mice (Charles River). The DG and the
545 SVZ were microdissected in 3% PBS-glucose. The cells of DG and the SVZ were then

546 separately (0.025% trypsin in PBS) for 5 min at 37°C. Cells were further dissociated in
547 DMEM/F12 medium by triturating the tissues with a fire-polished Pasteur pipette. Cells
548 suspensions were then centrifuged for 5 min at 1000*g* and the pellets were resuspended in
549 DMEM/F12 containing B27, N2, EGF, FGF and antibiotics. Cells were then incubated in non-
550 coated wells at 37°C and 5% CO_2 in a humidified environment.

551 **Synaptosome, PSD and PSW preparation**

552 Preparation of the fractions was performed as previously described[32,82]. Briefly, adult
553 hippocampi from 3 control mice or human biopsies (see below) were dissected and
554 synaptosomes were prepared by Ficoll density gradient centrifugation. Hippocampi were
555 homogenized using a 2 mL Dounce homogenizer in 5 mL of ice-cold homogenization buffer
556 (HB: 5 mM HEPES-KOH, pH 7.4, 320 mM sucrose). The homogenate was centrifuged at
557 3000*g* and the supernatant containing crude membrane was stored at 4°C (S1). The pellet
558 was resuspended in HB, re-pelleted at 3000*g* and the supernatant (S2) was pooled with S1.
559 S1 + S2 were then pelleted at 13,000*g*, washed and re-pelleted. The 'soft' pellet was
560 carefully resuspended in HB (avoiding as much as possible the lower pellet containing
561 mitochondria) and loaded on a 13/9/6% (4/1/1 mL, respectively) Ficoll gradient in HB. The
562 gradient was centrifuged at 86,800*g* (SW41 rotor) for 35 min at 4°C. 6/9% and 9/13%
563 interfaces contain synaptosomes. These fractions were pooled, washed, split into two
564 aliquots and repelleted in HB. One aliquot of synaptosomes was reserved and the other was
565 used to separate PSD and PSW fractions. The pellet was solubilised for 30 min at 4°C in a
566 final concentration of 20 mM Tris-HCl, pH 8.0 and 1% Triton X-100. The solution was then
567 centrifuged at 40,000*g* for 30 min at 4°C. The pellet containing an enrichment of PSD
568 proteins was solubilised in 100 µL 5% SDS and proteins in the supernatant were precipitated
569 by adding 10 volumes of acetone and incubating overnight at -20°C. The precipitates
570 corresponding to PSW proteins were then solubilised in 5% SDS.

571 **Electrophysiology**

572 Sagittal hippocampal slices were prepared from 6-weeks old control and CAR-CNS^{KO} mice
573 using standard techniques[83]. Recordings were conducted in an average of 3 slices per
574 animal. Each animal was anesthetised using isoflurane (Nicholas Piramal Limited) and
575 decapitated. Hippocampal slices were sectioned (350 µm-thick, vibratome Integraslice 7550)
576 and collected in oxygenated (95% O_2, 5% CO_2) ice-cold slicing buffer, (195 mM sucrose, 10
577 mM NaCl, 2.5 mM KCl, 1.25 mM NaH_2PO_4, 26 mM $NaHCO_3$, 15 mM glucose, 1 mM $CaCl_2$
578 and 2 mM $MgCl_2$) and gently transferred to a holding chamber. The holding chamber was
579 placed in a 32°C bath for the first 20 min and left at room temperature. Slices were
580 continuously supplied with oxygenated (95% O_2, 5% CO_2) artificial cerebrospinal fluid (ASCF:
581 110 mM NaCl, 1.2 mM KCl, 1.2 mM KH_2PO_4, 26 mM $NaHCO_3$, 10 mM glucose, 2 mM $CaCl_2$
582 and 2 mM $MgCl_2$). The recording chamber was continuously suffused with warm ACSF (35 ±
583 2°C) supplied with an atmosphere of 95% O_2 and 5% CO_2. Glass capillary microelectrodes
584 filled with ACSF were used to stimulate and record. Synaptic responses were evoked by
585 stimulating Schaffer collaterals. fEPSPs were recorded in the stratum radiatum of CA1 using
586 an AxoPatch 200A amplifier (Axon instruments, DIPSI). Signals were digitized (20 kHz
587 sampling rate) using Digidata and the Pclamp software (both from Axon instruments, DIPSI).
588 Baseline responses were obtained by stimulating (10-20 V during 0.2 ms; with a PPF
589 sequence delivered at intervals of 50 ms) the Schaffer collateral at 0.017 Hz (60 s intervals).
590 LTP was assessed for 1 h after a 10 min stable baseline response. To induce LTP, 3 trains
591 of HFS at 100 Hz (100 pulses for 1 s duration repeated 3 times at 10 s intervals) were
592 delivered, using the same stimulation intensity as for baseline stimulation. The fEPSP peak
593 amplitude (mV) data were compiled using the Pclamp software (both from Axon instruments,
594 DIPSI). fEPSP peak data were converted to percentages by setting the mean baseline
595 fEPSP peak data (fEPSP before applying HFS) to 100%. The PPF is expressed as the PPR
596 (ratio of the peak amplitude of the second over the first fEPSPs evoked at 50 ms interval).

597 **Adult neurogenesis**

598 We used a method consisting of combining the label of proliferating cells with a thymidine
599 analogue (BrdU or EdU) with neuronal markers. Briefly, mice received intraperitoneal
600 injections of BrdU or EdU or at a dose of 100 mg/kg body weight. Four weeks later, animals
601 were intracardiac perfused with 4% PFA/PBS and brains were processed as described in
602 immunohistochemistry and immunofluorescence section. EdU was then detected by adding
603 the Click-iT reaction buffer (from Click-iT EdU imaging kit, Invitrogen) according to the
604 manufacturer's protocol. Finally, neuronal labelling was performed by immunostaining of
605 neuronal (anti-NeuN or anti-PSA-NCAM). Quantification was performed by counting double-
606 positive cells. For this experiment, whole hippocampi were sliced and 1 section out of 8 was
607 used.

608 **Behaviour analyses**

609 Behavioural testing was performed between 10:00 to 14:00 h. In all experiments, we used
610 $CAR^{floxflox}$ animals as controls. Animals were subjected to a series of behavioural tests to
611 assess activity, anxiety, learning and memory, finishing with the most stressful procedures:
612 open-field, elevated-plus maze, Y maze, and water maze (spatial reference memory
613 procedure during 5 days, probe test on day 6 and visible platform procedure during 3 days)[84].
614 Animals were submitted to these different tasks and were then used for biochemical studies.
615 During each task, females and males were examined in parallel.

616 **Statistical analyses**

617 Data were analysed using Student's *t*-test for unpaired data, two-way ANOVA followed by
618 Tukey or Fisher post hoc test, Mann-Whitney test and chi-squared test (* *p*-value <0,05; ** *p*-
619 value <0,01; *** *p*-value <0,001 *vs.* control). See figure legends.

620 **Acknowledgments**

621 We thank the IGMM animal facility, Montpellier Rio Imaging for help with microscopy studies,
622 and Thierry Gostan for help with statistical analyses. We thank Stefano Musardo and Silvia

623 Pelucchi for technical help, F Tronche for the nestin-cre mice, and T Maurice for help with the
624 behavioural studies. SS and EJK are Inserm fellows.

625

626 **References**

627 1. Cavallaro, U. & Dejana, E. Adhesion molecule signalling: not always a sticky business. *Nature*
628 *reviews. Molecular cell biology* **12**, 189-197 (2011).

629 2. Togashi, H., Sakisaka, T. & Takai, Y. Cell adhesion molecules in the central nervous system.
630 *Cell adhesion & migration* **3**, 29-35 (2009).

631 3. Yamagata, M., Sanes, J.R. & Weiner, J.A. Synaptic adhesion molecules. *Curr Opin Cell Biol*
632 **15**, 621-632 (2003).

633 4. Lucas, S.M., Rothwell, N.J. & Gibson, R.M. The role of inflammation in CNS injury and
634 disease. *Br J Pharmacol* **147 Suppl 1**, S232-240 (2006).

635 5. Overk, C.R. & Masliah, E. Pathogenesis of synaptic degeneration in Alzheimer's disease and
636 Lewy body disease. *Biochem Pharmacol* **88**, 508-516 (2014).

637 6. Kohman, R.A. & Rhodes, J.S. Neurogenesis, inflammation and behavior. *Brain, behavior, and*
638 *immunity* **27**, 22-32 (2013).

639 7. Holmes, C.*, et al.* Systemic inflammation and disease progression in Alzheimer disease.
640 *Neurology* **73**, 768-774 (2009).

641 8. Valero, J., Mastrella, G., Neiva, I., Sanchez, S. & Malva, J.O. Long-term effects of an acute
642 and systemic administration of LPS on adult neurogenesis and spatial memory. *Frontiers in*
643 *neuroscience* **8**, 83 (2014).

644 9. Holmes, C. Review: systemic inflammation and Alzheimer's disease. *Neuropathology and*
645 *applied neurobiology* **39**, 51-68 (2013).

646 10. Heneka, M.T.*, et al.* Neuroinflammation in Alzheimer's disease. *The Lancet. Neurology* **14**,
647 388-405 (2015).

648 11. Freimuth, P., Philipson, L. & Carson, S.D. The coxsackievirus and adenovirus receptor.
649 *Current topics in microbiology and immunology* **323**, 67-87 (2008).

650 12. Cohen, C.J.*, et al.* The coxsackievirus and adenovirus receptor is a transmembrane
651 component of the tight junction. *Proc Natl Acad Sci U S A* **98**, 15191-15196 (2001).

652 13. Bergelson, J.M.*, et al.* Isolation of a common receptor for Coxsackie B viruses and
653 adenoviruses 2 and 5. *Science* **275**, 1320-1323 (1997).

654 14. Soudais, C.*, et al.* Canine adenovirus type 2 attachment and internalization: coxsackievirus-
655 adenovirus receptor, alternative receptors, and an RGD-independent pathway. *J Virol* **74**,
656 10639-10649 (2000).

657 15. Ekstrand, M.I.*, et al.* Molecular profiling of neurons based on connectivity. *Cell* **157**, 1230-1242
658 (2014).

659 16. Wu, Q., Clark, M.S. & Palmiter, R.D. Deciphering a neuronal circuit that mediates appetite.
660 *Nature* **483**, 594-U112 (2012).

661 17. Pivetta, C., Esposito, M.S., Sigrist, M. & Arber, S. Motor-Circuit Communication Matrix from
662 Spinal Cord to Brainstem Neurons Revealed by Developmental Origin. *Cell* **156**, 537-548
663 (2014).

664 18. Cubizolle, A.*, et al.* Corrective GUSB Transfer to the Canine Mucopolysaccharidosis VII Brain.
665 *Mol Ther* **22**, 762-773 (2014).

666 19. Senn, V.*, et al.* Long-range connectivity defines behavioral specificity of amygdala neurons.
667 *Neuron* **81**, 428-437 (2014).

668 20. Darvas, M., Wunsch, A.M., Gibbs, J.T. & Palmiter, R.D. Dopamine dependency for acquisition
669 and performance of Pavlovian conditioned response. *Proc Natl Acad Sci U S A* **111**, 2764-
670 2769 (2014).

671 21. Carter, M.E., Soden, M.E., Zweifel, L.S. & Palmiter, R.D. Genetic identification of a neural
672 circuit that suppresses appetite. *Nature* **503**, 111-+ (2013).

673 22. Beier, K.T.*, et al.* Circuit Architecture of VTA Dopamine Neurons Revealed by Systematic
674 Input-Output Mapping. *Cell* **162**, 622-634 (2015).

675 23. Schwarz, L.A.*, et al.* Viral-genetic tracing of the input-output organization of a central
676 noradrenaline circuit. *Nature* **524**, 88-92 (2015).

677 24. Bru, T., Salinas, S. & Kremer, E.J. An update on canine adenovirus type 2 and its vectors.
678 *Viruses* **2**, 2134-2153 (2010).

679 25. Salinas, S.*, et al.* CAR-associated vesicular transport of an adenovirus in motor neuron axons.
680 *PLoS Pathog* **5**, e1000442 (2009).

681 26. Coyne, C.B. & Bergelson, J.M. CAR: a virus receptor within the tight junction. *Adv Drug Deliv*
682 *Rev* **57**, 869-882 (2005).

683 27. Patzke, C.*, et al.* The coxsackievirus-adenovirus receptor reveals complex homophilic and
684 heterophilic interactions on neural cells. *J Neurosci* **30**, 2897-2910 (2010).

685 28. Soudais, C., Laplace-Builhe, C., Kissa, K. & Kremer, E.J. Preferential transduction of neurons
686 by canine adenovirus vectors and their efficient retrograde transport in vivo. *Faseb J* **15**, 2283-
687 2285 (2001).

688 29. Soudais, C., Skander, N. & Kremer, E.J. Long-term in vivo transduction of neurons throughout
689 the rat CNS using novel helper-dependent CAV-2 vectors. *Faseb J* **18**, 391-393 (2004).

690 30. Junyent, F. & Kremer, E.J. CAV-2 - why a canine virus is a neurobiologist's best friend. *Curr*
691 *Opin Pharma* **in press**(2015).

692 31. Persson, A., Fan, X., Widegren, B. & Englund, E. Cell type- and region-dependent coxsackie
693 adenovirus receptor expression in the central nervous system. *Journal of neuro-oncology* **78**,
694 1-6 (2006).

695 32. Garside, M.L.*, et al.* Molecular interactions of the plasma membrane calcium ATPase 2 at pre-
696 and post-synaptic sites in rat cerebellum. *Neuroscience* **162**, 383-395 (2009).

697 33. Tronche, F.*, et al.* Disruption of the glucocorticoid receptor gene in the nervous system results
698 in reduced anxiety. *Nat Genet* **23**, 99-103 (1999).

699 34. Chen, J.W.*, et al.* Cardiomyocyte-specific deletion of the coxsackievirus and adenovirus
700 receptor results in hyperplasia of the embryonic left ventricle and abnormalities of sinuatrial
701 valves. *Circ Res* **98**, 923-930 (2006).

702 35. Lepousez, G., Nissant, A. & Lledo, P.M. Adult neurogenesis and the future of the rejuvenating
703 brain circuits. *Neuron* **86**, 387-401 (2015).

704 36. Winner, B., Kohl, Z. & Gage, F.H. Neurodegenerative disease and adult neurogenesis. *Eur J*
705 *Neurosci* **33**, 1139-1151 (2011).

706 37. Dityatev, A., Bukalo, O. & Schachner, M. Modulation of synaptic transmission and plasticity by
707 cell adhesion and repulsion molecules. *Neuron glia biology* **4**, 197-209 (2008).

708 38. Ackermann, M. & Matus, A. Activity-induced targeting of profilin and stabilization of dendritic
709 spine morphology. *Nat Neurosci* **6**, 1194-1200 (2003).

710 39. Kang, H. & Schuman, E.M. Long-lasting neurotrophin-induced enhancement of synaptic
711 transmission in the adult hippocampus. *Science* **267**, 1658-1662 (1995).

712 40. Vincent, T., Pettersson, R.F., Crystal, R.G. & Leopold, P.L. Cytokine-mediated downregulation
713 of coxsackievirus-adenovirus receptor in endothelial cells. *J Virol* **78**, 8047-8058 (2004).

714 41. Gao, Y. & Lui, W.Y. Synergistic effect of interferon-gamma and tumor necrosis factor-alpha on
715 coxsackievirus and adenovirus receptor expression: an explanation of cell sloughing during
716 testicular inflammation in mice. *Biol Reprod* **90**, 59 (2014).

717 42. Houri, N., Huang, K.C. & Nalbantoglu, J. The Coxsackievirus and Adenovirus Receptor (CAR)
718 undergoes ectodomain shedding and regulated intramembrane proteolysis (RIP). *PLoS One*
719 **8**, e73296 (2013).

720 43. Zhou, L.*, et al.* The neural cell adhesion molecules L1 and CHL1 are cleaved by BACE1
721 protease in vivo. *J Biol Chem* **287**, 25927-25940 (2012).

722 44. Zhao, J.*, et al.* Beta-site amyloid precursor protein cleaving enzyme 1 levels become elevated
723 in neurons around amyloid plaques: implications for Alzheimer's disease pathogenesis. *J*
724 *Neurosci* **27**, 3639-3649 (2007).

725 45. Hensley, K. Neuroinflammation in Alzheimer's disease: mechanisms, pathologic
726 consequences, and potential for therapeutic manipulation. *Journal of Alzheimer's disease :*
727 *JAD* **21**, 1-14 (2010).

728 46. Yamamoto, M.*, et al.* Interferon-gamma and tumor necrosis factor-alpha regulate amyloid-beta
729 plaque deposition and beta-secretase expression in Swedish mutant APP transgenic mice.
730 *Am J Pathol* **170**, 680-692 (2007).

731 47. Liu, G.*, et al.* Cell adhesion molecules contribute to Alzheimer's disease: multiple pathway
732 analyses of two genome-wide association studies. *J Neurochem* **120**, 190-198 (2012).

733 48. Wondolowski, J. & Dickman, D. Emerging links between homeostatic synaptic plasticity and
734 neurological disease. *Front Cell Neurosci* **7**, 223 (2013).

735 49. Scheff, S.W., Price, D.A., Schmitt, F.A. & Mufson, E.J. Hippocampal synaptic loss in early
736 Alzheimer's disease and mild cognitive impairment. *Neurobiology of aging* **27**, 1372-1384
737 (2006).

738 50. Oddo, S.*, et al.* Triple-transgenic model of Alzheimer's disease with plaques and tangles:
739 intracellular Abeta and synaptic dysfunction. *Neuron* **39**, 409-421 (2003).

740 51. Bories, C.*, et al.* Sex-dependent alterations in social behaviour and cortical synaptic activity
741 coincide at different ages in a model of Alzheimer's disease. *PLoS One* **7**, e46111 (2012).

742 52. Janelsins, M.C.*, et al.* Early correlation of microglial activation with enhanced tumor necrosis
743 factor-alpha and monocyte chemoattractant protein-1 expression specifically within the
744 entorhinal cortex of triple transgenic Alzheimer's disease mice. *J Neuroinflammation* **2**, 23
745 (2005).

746 53. Marcello, E.*, et al.* SAP97-mediated local trafficking is altered in Alzheimer disease patients'
747 hippocampus. *Neurobiology of aging* **33**, 422 e421-410 (2012).

748 54. Liao, Y.F., Wang, B.J., Cheng, H.T., Kuo, L.H. & Wolfe, M.S. Tumor necrosis factor-alpha,
749 interleukin-1beta, and interferon-gamma stimulate gamma-secretase-mediated cleavage of
750 amyloid precursor protein through a JNK-dependent MAPK pathway. *J Biol Chem* **279**, 49523-
751 49532 (2004).

752 55. Seki, T., Namba, T., Mochizuki, H. & Onodera, M. Clustering, migration, and neurite formation
753 of neural precursor cells in the adult rat hippocampus. *J Comp Neurol* **502**, 275-290 (2007).

754 56. Schmidt-Hieber, C., Jonas, P. & Bischofberger, J. Enhanced synaptic plasticity in newly
755 generated granule cells of the adult hippocampus. *Nature* **429**, 184-187 (2004).

756 57. Mongiat, L.A. & Schinder, A.F. Adult neurogenesis and the plasticity of the dentate gyrus
757 network. *Eur J Neurosci* **33**, 1055-1061 (2011).

758 58. Murphy, K.J., O'Connell, A.W. & Regan, C.M. Repetitive and transient increases in
759 hippocampal neural cell adhesion molecule polysialylation state following multitrial spatial
760 training. *J Neurochem* **67**, 1268-1274 (1996).

761 59. Sandi, C. Stress, cognitive impairment and cell adhesion molecules. *Nat Rev Neurosci* **5**, 917-
762 930 (2004).

763 60. Lopez-Fernandez, M.A.*, et al.* Upregulation of polysialylated neural cell adhesion molecule in
764 the dorsal hippocampus after contextual fear conditioning is involved in long-term memory
765 formation. *J Neurosci* **27**, 4552-4561 (2007).

766 61. Foley, A.G.*, et al.* Consolidation of memory for odour-reward association requires transient
767 polysialylation of the neural cell adhesion molecule in the rat hippocampal dentate gyrus. *J*
768 *Neurosci Res* **74**, 570-576 (2003).

769 62. Ronn, L.C., Berezin, V. & Bock, E. The neural cell adhesion molecule in synaptic plasticity and
770 ageing. *International journal of developmental neuroscience : the official journal of the*
771 *International Society for Developmental Neuroscience* **18**, 193-199 (2000).

63. Dityatev, A. & Schachner, M. Extracellular matrix molecules and synaptic plasticity. *Nat Rev Neurosci* **4**, 456-468 (2003).

64. Bonfanti, L. PSA-NCAM in mammalian structural plasticity and neurogenesis. *Progress in neurobiology* **80**, 129-164 (2006).

65. Excoffon, K.J., Gansemer, N., Traver, G. & Zabner, J. Functional effects of coxsackievirus and adenovirus receptor glycosylation on homophilic adhesion and adenoviral infection. *J Virol* **81**, 5573-5578 (2007).

66. Seidenfaden, R., Krauter, A. & Hildebrandt, H. The neural cell adhesion molecule NCAM regulates neuritogenesis by multiple mechanisms of interaction. *Neurochem Int* **49**, 1-11 (2006).

67. Shi, Y. & Ethell, I.M. Integrins control dendritic spine plasticity in hippocampal neurons through NMDA receptor and Ca2+/calmodulin-dependent protein kinase II-mediated actin reorganization. *J Neurosci* **26**, 1813-1822 (2006).

68. Burgess, A.*, et al.* Polysialic acid regulates the clustering, migration, and neuronal differentiation of progenitor cells in the adult hippocampus. *Dev Neurobiol* **68**, 1580-1590 (2008).

69. Parks, A.L. & Curtis, D. Presenilin diversifies its portfolio. *Trends in genetics : TIG* **23**, 140-150 (2007).

70. Dephoure, N.*, et al.* A quantitative atlas of mitotic phosphorylation. *Proc Natl Acad Sci U S A* **105**, 10762-10767 (2008).

71. Spalding, K.L.*, et al.* Dynamics of hippocampal neurogenesis in adult humans. *Cell* **153**, 1219-1227 (2013).

72. D'Arcangelo, G.*, et al.* A protein related to extracellular matrix proteins deleted in the mouse mutant reeler. *Nature* **374**, 719-723 (1995).

73. Rodriguez, J.J.*, et al.* Impaired adult neurogenesis in the dentate gyrus of a triple transgenic mouse model of Alzheimer's disease. *PLoS One* **3**, e2935 (2008).

74. Greten-Harrison, B.*, et al.* alphabetagamma-Synuclein triple knockout mice reveal age-dependent neuronal dysfunction. *Proc Natl Acad Sci U S A* **107**, 19573-19578 (2010).

75. Salinas, S.*, et al.* Disruption of the coxsackievirus and adenovirus receptor-homodimeric interaction triggers lipid microdomain- and dynamin-dependent endocytosis and lysosomal targeting. *J Biol Chem* **289**, 680-695 (2014).

76. Vina, J. & Lloret, A. Why women have more Alzheimer's disease than men: gender and mitochondrial toxicity of amyloid-beta peptide. *Journal of Alzheimer's disease : JAD* **20 Suppl 2**, S527-533 (2010).

77. Li, R. & Singh, M. Sex differences in cognitive impairment and Alzheimer's disease. *Frontiers in neuroendocrinology* **35**, 385-403 (2014).

78. Ooishi, Y.*, et al.* Modulation of synaptic plasticity in the hippocampus by hippocampus-derived estrogen and androgen. *J Steroid Biochem Mol Biol* **131**, 37-51 (2012).

79. Roepke, T.A., Ronnekleiv, O.K. & Kelly, M.J. Physiological consequences of membrane-initiated estrogen signaling in the brain. *Front Biosci* **16**, 1560-1573 (2011).

80. Vindrieux, D.*, et al.* Coxsackie and adenovirus receptor is a target and a mediator of estrogen action in breast cancer. *Endocrine-related cancer* **18**, 311-321 (2011).

81. Guo, W., Patzlaff, N.E., Jobe, E.M. & Zhao, X. Isolation of multipotent neural stem or progenitor cells from both the dentate gyrus and subventricular zone of a single adult mouse. *Nature protocols* **7**, 2005-2012 (2012).

82. Khaing, Z.Z., Fidler, L., Nandy, N. & Phillips, G.R. Structural stabilization of CNS synapses during postnatal development in rat cortex. *J Neurochem* **98**, 471-480 (2006).

83. Chafai, M., Corbani, M., Guillon, G. & Desarmenien, M.G. Vasopressin inhibits LTP in the CA2 mouse hippocampal area. *PLoS One* **7**, e49708 (2012).

821 84. Maurice, T., *et al.* Cystine accumulation in the CNS results in severe age-related memory
822 deficits. *Neurobiology of aging* **30**, 987-1000 (2009).

823

824

825 **Figures and legends**

826 **Figure 1: CAR in axons and on the soma of cells in the hippocampus, as well as at**
827 **presynaptic termini**

828 **(**A) Representative image of anti-CAR immunohistochemistry (IHC) in a coronal section from
829 the brain of a healthy adult mouse. Solid black arrows show intense CAR staining in layer I
830 and near layer IV/V of the cerebral cortex and posterior corpus callosum. (**B**) Magnification of
831 the boxed area in **A** showing CAR labelling in the hippocampus. Soma of cells in the dentate
832 gyrus (DG) subgranular zone (SGZ) and and granular cell layer (GCL) (solid black arrows)
833 and showing axons projecting from the entorhinal cortex (black arrows) and in the stratum
834 lucidum (SLu) (open black arrows). (**C**) Magnification of boxed area in **B** showing IHC and
835 immunofluorescent (IF) staining of CAR staining (black and white arrows, respectively) in
836 fibres within the SLu. (**D**) Magnification of boxed area in B showing IHC and IF staining
837 (black and white arrowheads, respectively) of CAR staining on the soma and projections
838 from cells in the SGZ and GCL. (**E**) CAR is enriched in pre-synaptic fractions in the mature
839 mouse brain. Synaptosomes from adult mouse brain were screened for CAR. Representative
840 immunoblots showing input, synaptosome, post-synaptic density (PSD), and presynaptic web
841 and vesicles (PSW+V). Synaptophysin (SYP) was used as a marker for the PSW+V; NR1
842 and PSD95 as markers for the PSD; and NeuN as a somal marker. (**F**) Hippocampal neurons
843 (≥ DIV14) were co-stained for endogenous CAR (in magenta) and with the presynaptic
844 marker SYP (in green). Arrows show double-positives structures. (**G**) Hippocampal neurons
845 (≥ DIV21) were co-stained for endogenous CAR (in magenta) and MAP2 (in green) to
846 visualise dendritic spines (white arrows). Scale bars: (**A**) 1 mm; (**B**) 100 µm; (**C**) 50 µm; (**F** &
847 **G**) 10 µm.

848 **Figure 2: CAR involvement in adult neurogenesis**

849 (**A**) Immunoblot analyses from 2-month-old control (CT) and CAR-CNS^{KO} mice showed
850 deletion of CAR (~46 kDa) in the brain, while expression in skeletal muscle and liver is
851 similar to controls. β-tubulin (~50 kDa) was used as a loading control. (**B**) Cresyl violet and

luxol fast blue coloration of 2-month-old CT and CAR-CNS^{KO} brains. Coronal brain sections of the DG: boxed region is magnified in the panel on the right to show the GCL. (**C**) Average area of the GCL in CT and CAR-CNS^{KO} mice. (**D**) The GCL of the DG of 2-month-old CT mice stained with anti-CAR, anti-PSA-NCAM and DAPI staining of nuclei; (**E**) The SLu of the DG of 2-month-old CT mice stained with anti-CAR, anti-PSA-NCAM and DAPI staining of nuclei; (**F**) The GCL of the DG of 2-month-old CT mice stained with anti-CAR, anti-NeuN and DAPI staining of nuclei. Boxed regions in the upper left panel in **D-F** are expanded in the upper right panels. White arrows show overlapping expression. (**G-J**) Adult neurogenesis in CAR-CNS^{KO} mice: (**G-H**) Quantification of proliferative cells (incorporation of a thymidine analogue) in the SGZ of the DG in CT and CAR-CNS^{KO} mice at 1 and 28 days post-injection. (**I**) Percentage of new neurons/DG ((EdU^{+} + NeuN^{+} cells/EdU^{+} cells) x 100)) CT and CAR-CNS^{KO} mice 28 days post-injection. (**J**) Percentage of immature neurons/DG ((EdU^{+} + PSA-NCAM^{+} cells/EdU^{+} cells) x 100)) CT and CAR-CNS^{KO} mice 28 days post-injection. Results are expressed as means ± SEM and the number of animals in groups is indicated within the columns. * *p*-value <0.05, ** *p*-value <0.001. Scale bars: **B** right panels = 20 µm; **D – F** upper left panels = 50 µm; **D – F** lower and right panels = 10 µm.

Figure 3: CAR loss of function affects synapse homeostasis

(**A**) Quantification of colocalisation between synaptophysin (SYP) and CAR when neuronal depolarisation is induced by 90 mM KCl (**B**) Quantification of colocalisation between SYP and CAR after incubation with BDNF. Each condition is the percentage of synapses (SYP^{+} structures) containing CAR and is expressed as means ± SEM of 3 independent experiments. Greater than 200 SYP^{+} structures were analysed at each condition. (**C** - **D**) Effect of CAR loss of function on synapse content in the hippocampus: Quantification of immunoblots for synaptic proteins: relevant proteins and respective representative immunoblots are shown under the columns. The intensity of the bands was quantified and normalised to β-tubulin levels for each marker. NB: some filters were used for more than one protein and therefore the same control β-tubulin bands were used to compare the levels of

879 different synaptic proteins. Results are expressed as percentage in control mice. As
880 differences appeared between sexes, we separated males (**C**) and females (**D**). n = the
881 number of animals.

882 **Figure 4: Effect of CAR loss of function on neurotransmission**

883 (**A**) fEPSPs recordings were performed in hippocampal slices from 6 to 8-week-old female
884 control (CT) and CAR-CNSKO mice. Representative recordings of the fEPSPs before (black)
885 and after (red) HFS. The LTP (comparison between red and black traces) is shown. (**B**) PPR
886 in male CT and CAR-CNSKO mice. (**C**) PPR in female CT and CAR-CNSKO mice. Results
887 are expressed as the ratio between the fEPSP peaks of the response 1 and 2. These
888 measures were performed before (basal activity) and after induction of LTP (60 min post
889 HFS). The number of slices in each group is indicated within the columns. (**D**) LTP induction
890 in male CT and CAR-CNSKO mice. (**E**) LTP induction in female CT and CAR-CNSKO mice.
891 LTP was assessed for 1 h after a 10 min stable baseline response. fEPSP peak data were
892 converted to percentages by setting the baseline fEPSP peak data to 100%. Results are
893 expressed as means ± SEM. Data were analysed using Student's t-test for unpaired data (**B**-
894 **C**) and two-way ANOVA followed by a Fisher LSD test (**D**-**E**) * p-value <0.05, ** p-value
895 <0.01 vs. control).

896 **Figure 5: CAR loss of function affects behaviour**

897 Behavioural analyses of: (**A**) Anxiety was measured using their ability to explore the open
898 arms of an elevated plus maze. The apparatus consisted of a plus-shape maze with two
899 opposite open (23.5 x 8 cm) and enclosed arms (23.5 x 8 x 20 cm high). The arms extended
900 from a central platform (8 x 8 cm) and the maze was elevated to a height of 50 cm above the
901 floor. Each mouse was placed at the centre of the maze and could freely explore for 10 min.
902 The time spent in open arms was recorded. Results were expressed as total time spent in
903 the open arms (10 min) and the readout was the time spent in the open arms. We found no
904 difference between males and females, and therefore the results are pooled. (**B**) Spatial
905 working memory was recorded as described in a three-arm maze (40-cm long, 13-cm high,

3-cm wide at the bottom, 10-cm wide at the top) converging at an equal angle (labelled A, B, and C). Each mouse was placed at the end of arm "C" and allowed to move freely through the maze during an 8 min session. The sequence and number of arm entries were recorded. Results are expressed as the percentage of alternations (defined as entries into all three arms on consecutive occasions, i.e., ACB, ABC, BCA…). The percentage of alternation was calculated as the ratio of actual to possible alternations (defined as the total number of arm entries minus two), multiplied by 100. We found no difference between males and females, and therefore the results are pooled. (**C**) The Morris water maze was a circular pool (Ø 150 cm, height 30 cm), arbitrarily divided into four quadrants. The water temperature (21 ± 1°C), light intensity, external cues in the room, and water opacity were rigorously controlled. A hidden platform (Ø 10 cm) was immersed beneath the water surface in the centre of one of the quadrants (termed the training quadrant). Reference memory training consisted of 3 swims/day during 5 days with 20 min inter-trial time interval. To find the platform, animals were allowed to swim for 90 s and to use visual extra-maze cues. Mice were then left on the platform for 20 s. The median latency was calculated for each training day and expressed as mean ± S.E.M. On day 6, a probe test was performed to measure the memory retention. The platform was removed and each animal was allowed to freely swim for 60 s. The time spent in the training quadrant was determined using Videotrack software (Viewpoint). We found no difference between males and females, and therefore the results are pooled. (**D & E**) Memory retention in CAR-CNS^{KO} mice: The probe test was performed 1 day after the last training session in a single 60 s swim without the platform. The presence in the training quadrant was analysed over the chance level (red line at 15 s). There were notable difference between the male and female mice and therefore the results are presented separately. All the results are expressed as means ± SEM and the number of animals in groups is indicated within the columns of results. Data were analysed using chi-squared test (**B**); two-way ANOVA followed by a Tukey post hoc test (**C**) and Student's *t*-test for unpaired data (**A, D, E**) (* *p*-value <0.05, ** *p*-value <0.01, *** *p*-value <0.001 *vs. control* (CT)).

933 **Figure 6: Downregulation of CAR by secretases and pro-inflammatory cytokines**

934 (**A**) Primary murine hippocampal neuron cultures were mock- or ionomycin-treated to induce
935 secretase activation. Supernatant and cells were collected separately and assayed for the
936 presence of CAR using an anti-CAR that recognizes the extracellular domains.
937 Representative immunoblot of three independent experiments. β-tubulin was used as a
938 loading control. (**B**) Primary cultures of murine hippocampal neurons were incubated with
939 FK^{CAV}, as a control for CAR degradation[75] or increasing concentrations of TNF-α and INF-γ
940 for 72 h. Representative immunoblot showing CAR levels, with β-tubulin used as a loading
941 control. (**C**) Primary cultures of adult NPCs were incubated with FK^{CAV} or increasing
942 concentrations of TNF-α and INF-γ for 72 h. Representative immunoblot showing CAR levels,
943 with β-tubulin used as a loading control. (**D**) Quantitative analyses of three independent
944 experiments of CAR loss in primary cultures of murine hippocampal neurons. (**E**) Effect of
945 systemic inflammation triggered by intraperitoneal injection of LPS in healthy mice. LPS
946 injections (top panels) triggers CAR loss from SGZ and GCL (left hand panels) and SLu of
947 the DG (middle panels) compared to PBS-injected mice (bottom row). Representative IHC
948 analyses of CAR and PSA-NCAM in the DG show loss of CAR in LPS-injected mice
949 compared to PBS-injected mice 1 week post-injection. Compared to PBS-injected controls,
950 PSA-NCAM staining is unaffected following LPS injections (right panels). Scale bars = 50
951 µm.

952 **Figure 7: CAR loss in human and murine Alzheimer's disease hippocampus**

953 Representative immunoblots of CAR levels in proteins extracted from the hippocampi from
954 **(A)** 5-8-month-old (top panel) and 16-20-month-old (bottom panel) WT and 3xTgAD mice.
955 **(B)** Quantification of CAR levels in the blots from (**A**) in 3xTgAD mice. CAR levels were
956 normalised to β-tubulin. Number of samples is indicated within the columns. (**C**) *Cxadr* mRNA
957 levels in hippocampi of wild type and 3xTgAD mice. mRNA levels were quantified by qRT-
958 PCR and normalized to GAPDH levels. (**D**) Wild type and 3xTgAD mice were injected in the
959 peritoneal cavity with LPS and sacrificed 7 weeks postinjection. Representative images of

960 CAR IHC in coronal sections containing the GCL (top row) and SLu (bottom row) from mice ±
961 LPS injections. (**E**) Quantification of CAR^+ cells in the GCL from WT and 3xTgAD mice
962 injected in the peritoneal cavity with LPS and sacrificed 7 weeks postinjection. Quantification
963 was performed using ImageJ. A 500-µm-long segmented line (10 pixel width) was drawn
964 through the middle of the GCL and signal intensity along that line was plot. Each peak above
965 the threshold (80 in the grey scale 0-255) corresponds to a neuron (≥6 sections from each of
966 the four mice were used). (**F**) Protein extracts from the hippocampus from AD patients and
967 age-matched controls were subjected to immunoblotting and CAR level were normalised to
968 β-tubulin. (**G**) Quantitative analyses of CAR and VGLUT levels in (**F**). Results are expressed
969 as means ± SEM, and the number of samples is indicated within the columns. Data were
970 analysed using Student's *t*-test for unpaired data. **p*-value <0.05, ** *p*-value <0.01, and ****
971 *p*-value <0.0001.

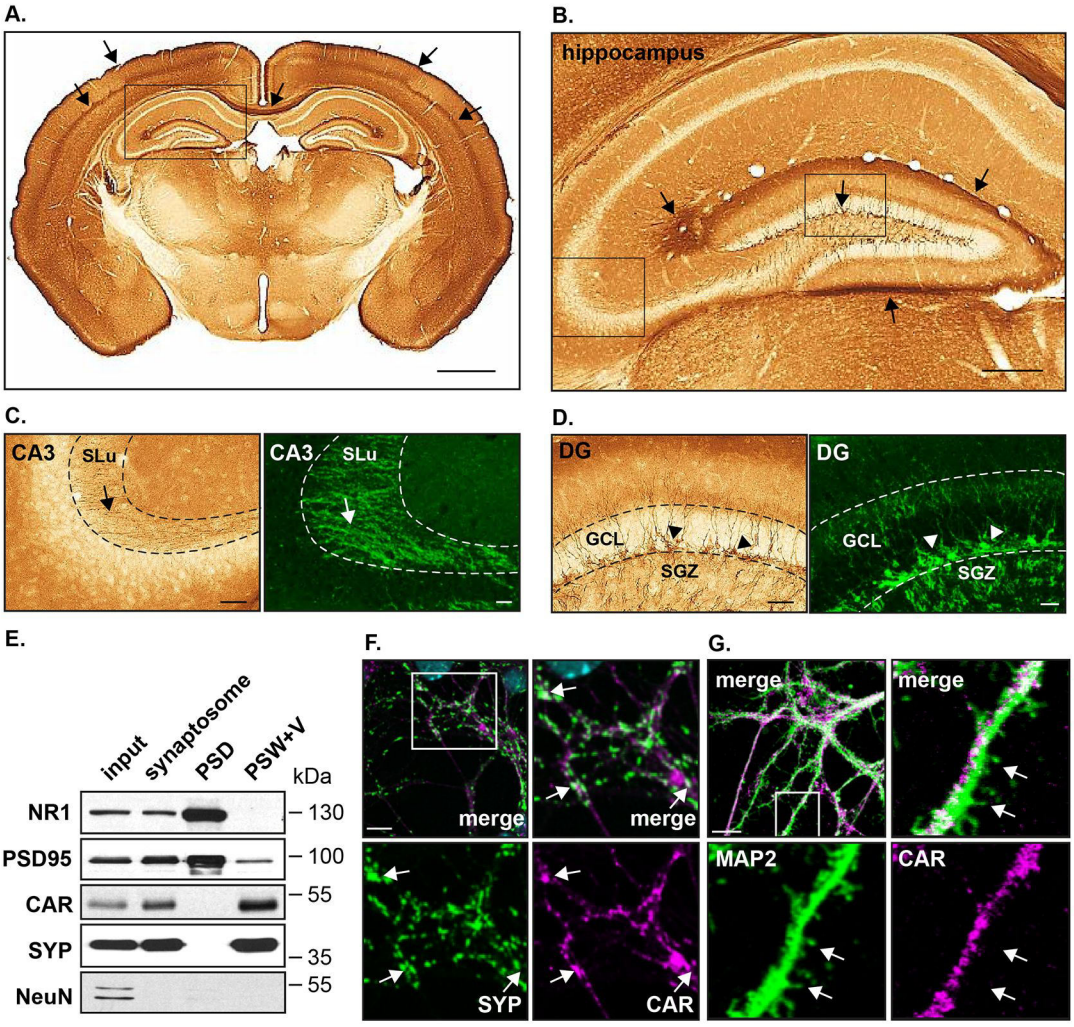
A.
B.
hippocampus
C.
CA3
SLu
CA3
SLu
D.
DG
GCL
SGZ
DG
GCL
SGZ
E.
input
synaptosome
PSD
PSW+V
kDa
NR1
130
PSD95
100
CAR
55
SYP
35
NeuN
55
F.
merge
merge
SYP
CAR
G.
merge
merge
MAP2
CAR

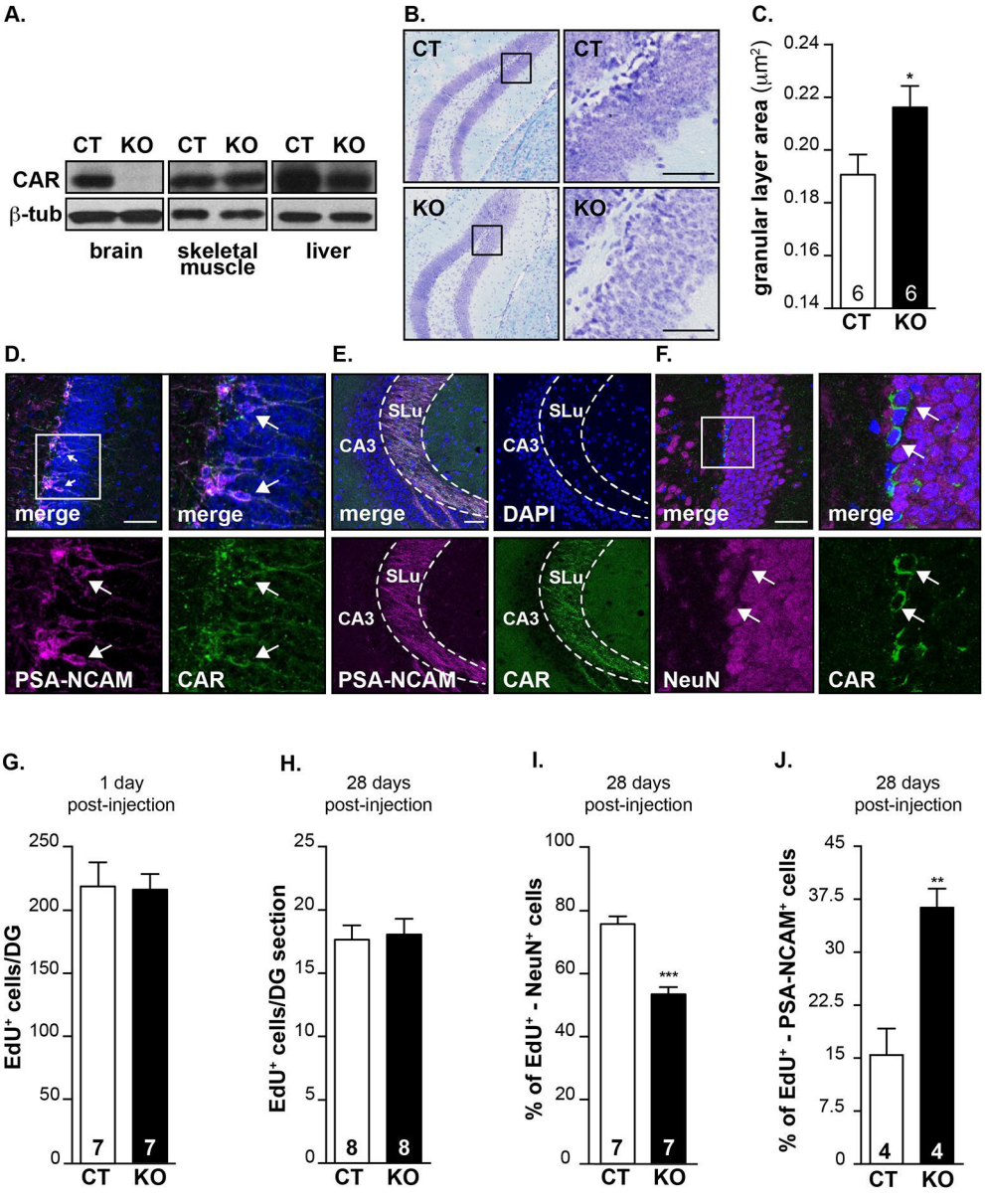
A.
CT KO CT KO CT KO
CAR
β-tub
brain
skeletal muscle
liver
B.
CT
CT
KO
KO
C.
granular layer area (μm²)
0.24
0.22
0.20
0.18
0.16
0.14
*
6
6
CT KO
D.
E.
F.
merge
merge
SLu
CA3
merge
SLu
CA3
DAPI
merge
merge
PSA-NCAM
CAR
SLu
CA3
PSA-NCAM
SLu
CA3
CAR
NeuN
CAR
G.
1 day post-injection
EdU⁺ cells/DG
250
200
150
100
50
0
7
7
CT KO
H.
28 days post-injection
EdU⁺ cells/DG section
25
20
15
10
5
0
8
8
CT KO
I.
28 days post-injection
% of EdU⁺ - NeuN⁺ cells
100
80
60
40
20
0
***
7
7
CT KO
J.
28 days post-injection
% of EdU⁺ - PSA-NCAM⁺ cells
45
37.5
30
22.5
15
7.5
0
**
4
4
CT KO

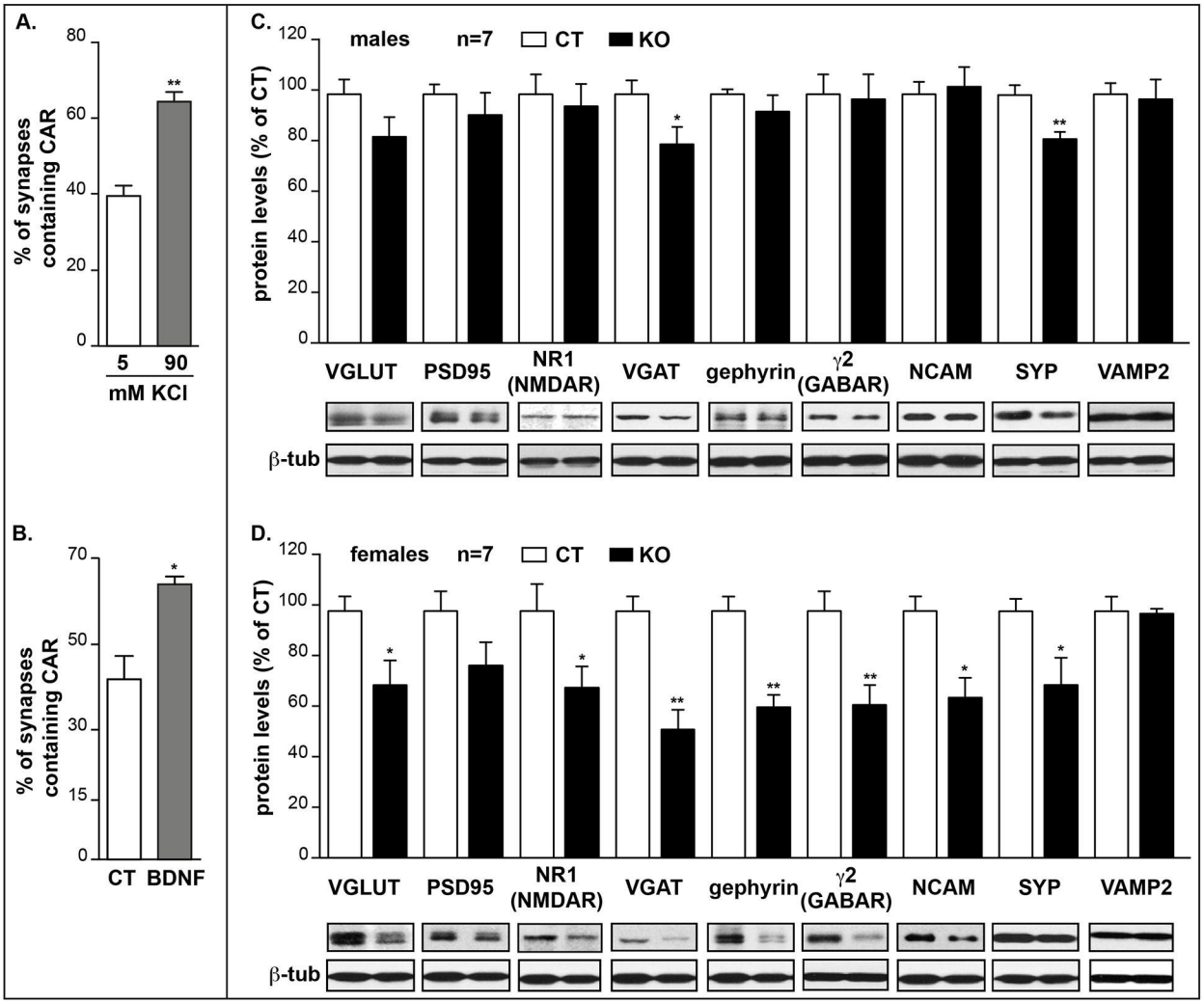
A.
% of synapses containing CAR
80
60
40
20
0
**
5
90
mM KCl
B.
% of synapses containing CAR
70
50
30
15
0
*
CT
BDNF
C.
males
n=7
CT
KO
protein levels (% of CT)
120
100
80
60
40
20
0
*
**
VGLUT
PSD95
NR1 (NMDAR)
VGAT
gephyrin
γ2 (GABAR)
NCAM
SYP
VAMP2
β-tub
D.
females
n=7
CT
KO
protein levels (% of CT)
120
100
80
60
40
20
0
*
**
VGLUT
PSD95
NR1 (NMDAR)
VGAT
gephyrin
γ2 (GABAR)
NCAM
SYP
VAMP2
β-tub

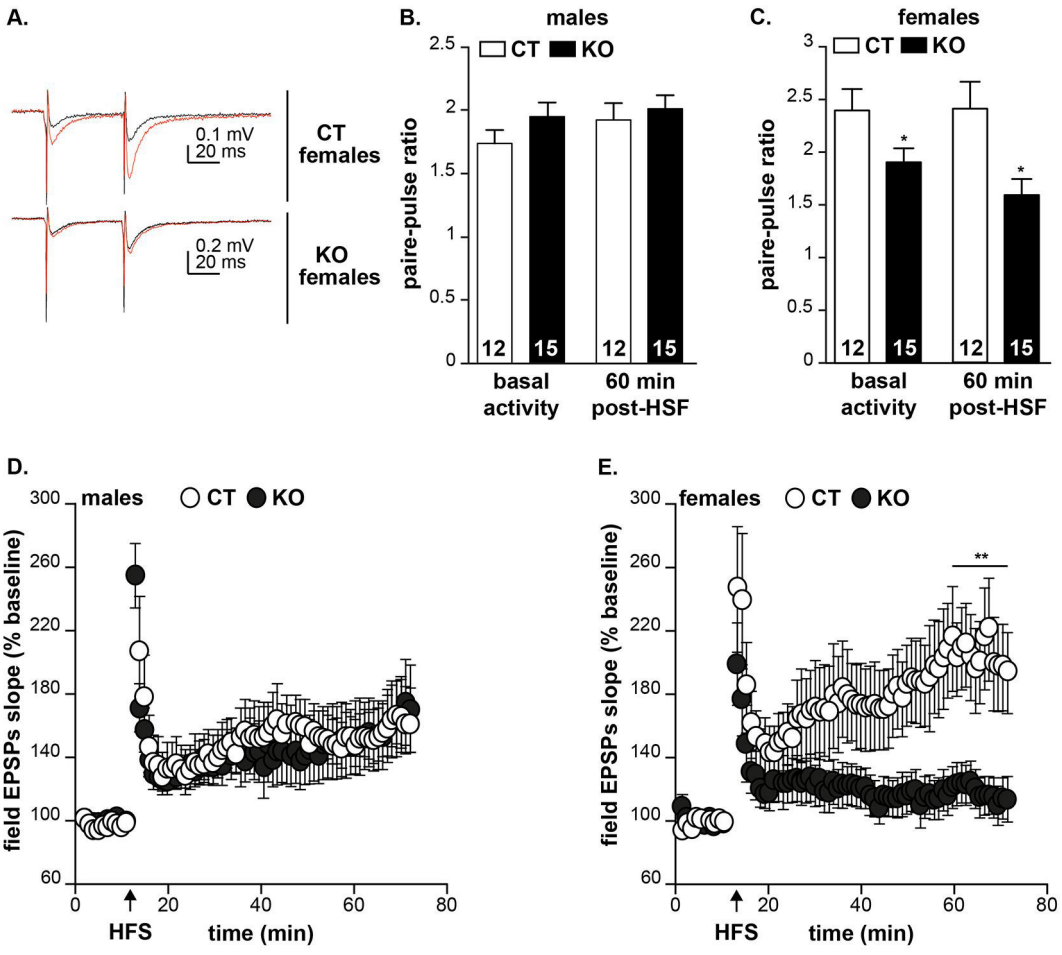
A.
0.1 mV
20 ms
CT
females
0.2 mV
20 ms
KO
females
B.
males
CT KO
paire-pulse ratio
2.5
2
1.5
1
0.5
0
12
15
12
15
basal
activity
60 min
post-HSF
C.
females
CT KO
paire-pulse ratio
3
2.5
2
1.5
1
0.5
0
*
*
12
15
12
15
basal
activity
60 min
post-HSF
D.
males
CT KO
field EPSPs slope (% baseline)
300
260
220
180
140
100
60
0
20
40
60
80
HFS
time (min)
E.
females
CT KO
field EPSPs slope (% baseline)
**
300
260
220
180
140
100
60
0
20
40
60
80
HFS
time (min)

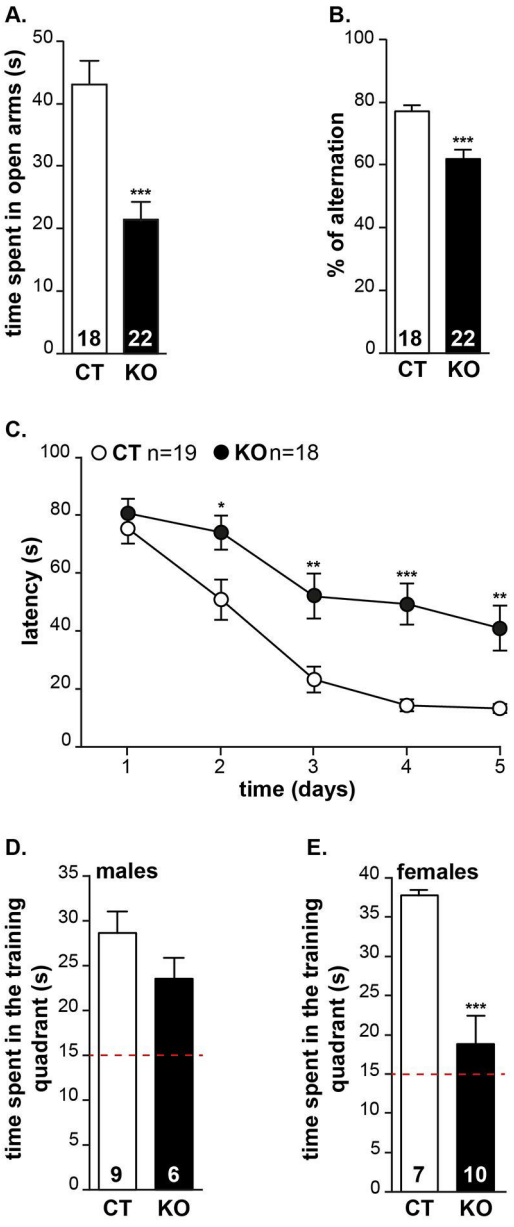
A.
time spent in open arms (s)
50
40
30
20
10
0
***
18
22
CT
KO
B.
% of alternation
100
80
60
40
20
0
***
18
22
CT
KO
C.
CT n=19
KO n=18
latency (s)
100
80
60
40
20
0
*
**
***
**
1
2
3
4
5
time (days)
D.
males
time spent in the training quadrant (s)
35
30
25
20
15
10
5
0
9
6
CT
KO
E.
females
time spent in the training quadrant (s)
40
35
30
25
20
15
10
5
0
***
7
10
CT
KO

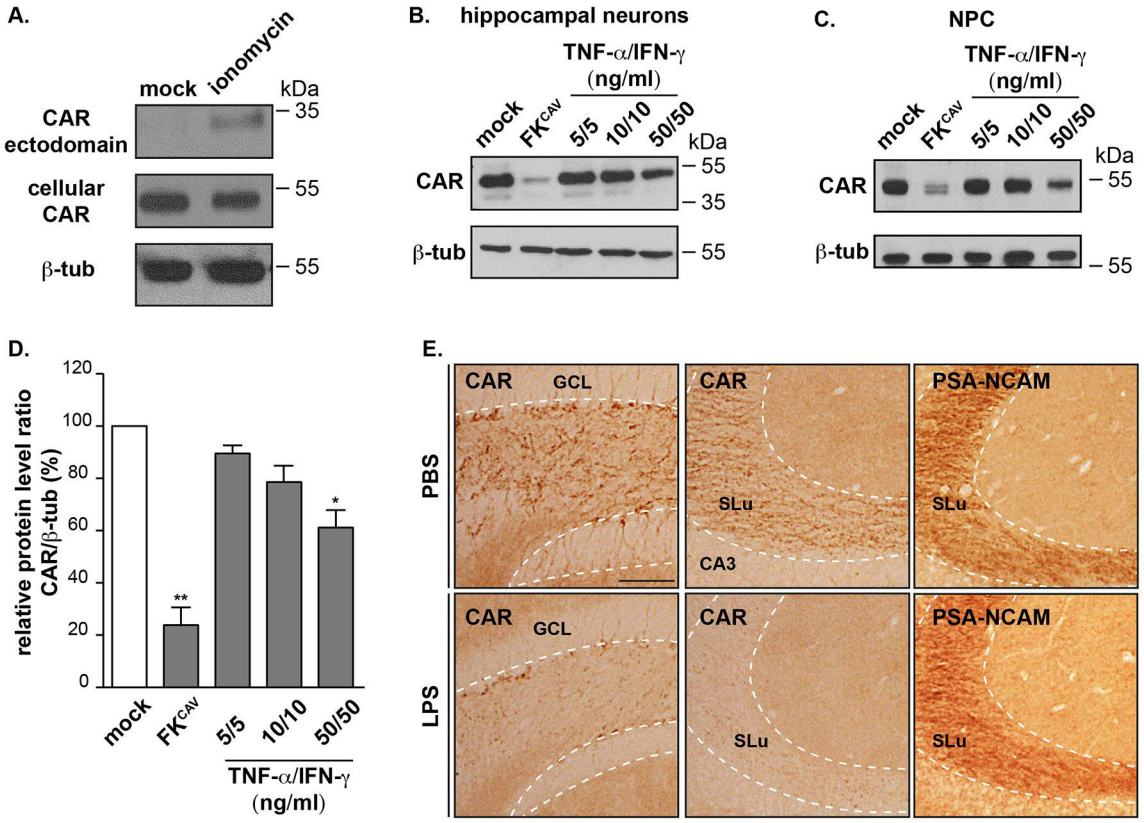
A.
mock
ionomycin
kDa
CAR ectodomain
35
cellular CAR
55
β-tub
55
B.
hippocampal neurons
TNF-α/IFN-γ (ng/ml)
mock
FKCAV
5/5
10/10
50/50
kDa
CAR
55
35
β-tub
55
C.
NPC
TNF-α/IFN-γ (ng/ml)
mock
FKCAV
5/5
10/10
50/50
kDa
CAR
55
β-tub
55
D.
relative protein level ratio CAR/β-tub (%)
120
100
80
60
40
20
0
**
*
mock
FKCAV
5/5
10/10
50/50
TNF-α/IFN-γ (ng/ml)
E.
PBS
LPS
CAR
GCL
CAR
SLu
CA3
PSA-NCAM
SLu
CAR
GCL
CAR
SLu
PSA-NCAM
SLu

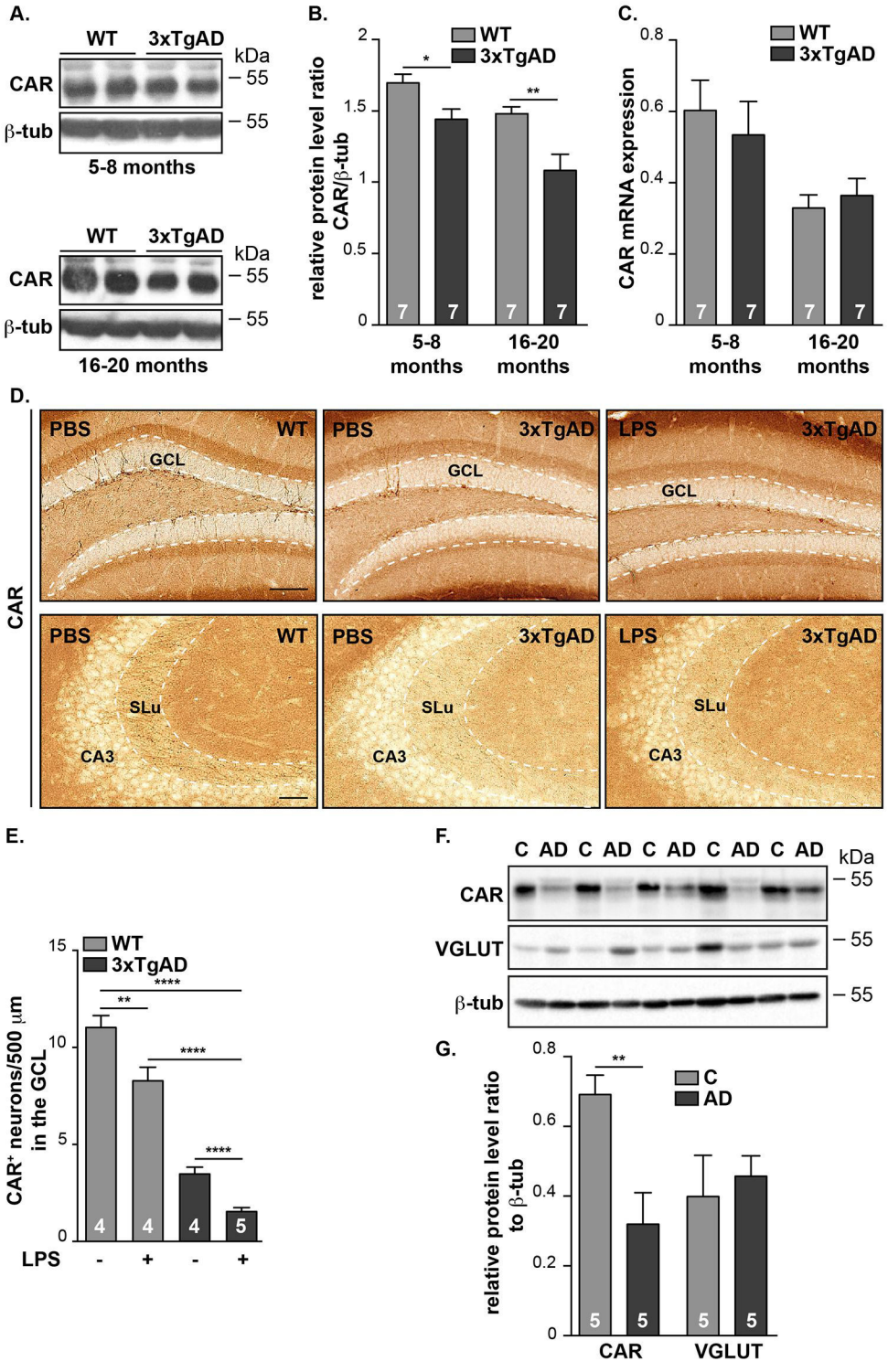
A.
WT
3xTgAD
kDa
CAR
β-tub
– 55
– 55
5-8 months
16-20 months
B.
WT
3xTgAD
relative protein level ratio CAR/β-tub
5-8 months
16-20 months
C.
CAR mRNA expression
D.
CAR
PBS
LPS
GCL
SLu
CA3
E.
CA⁺ neurons/500 μm in the GCL
LPS
F.
C AD C AD C AD C AD C AD
VGLUT
G.
relative protein level ratio to β-tub
C
AD
CAR
VGLUT

Supplementary Figure Legends:

Figure S1: **CAR subcellular location**

A. CAR is enriched in pre-synaptic fractions in the mature human brain. Synaptosomes isolation from adult human cortex were screened for CAR levels by immunblotting. A representative immunoblot showing input, synaptosome, pre-synaptic web and vesicles (PSW+V), and post-synaptic density (PSD). Synaptophysin (SYP) was used as a marker for the PSW+V; PSD95 as markers for the PSD. **B.** CAR is located in synapses. DIV14 murine hippocampal neurons were labelled for glutamatergic and GABAergic synapses using VGLUT and VGAT, respectively. Colocalization (white arrows) with PSD95 indicates synapses. CAR colocalizes with VGLUT and VGAT, showing that CAR was expressed in excitatory and inhibitory synapses. Scale bar = 15 µm.

Figure S2: **Generation and cahracterization of CAR-CNS^{KO} mice**.

A. Deletion of *Cxadr* in the CNS. (Left) Schematic representation showing the strategy used to obtain CAR-CNS^{KO} mice. CAR$^{flox/flox}$ mice were crossed with nestin-cre mice to obtain CAR$^{flox/wt}$ nestin-cre animals. These mice were then crossed with CAR$^{flox/flox}$ to obtain CAR-CNS^{KO} and CT (control) (CARflox/flox) animals. (Right) Example of genotyping results using primers flanking the *Cxadr* exon 2 region. **B.** Immunohistochemistry of CAR expression in CT and CAR-CNS^{KO} mice. **C.** Brain morphology revealed by luxol blue staining of CT and CAR-CNS^{KO} mice showing no significant difference. **D.** Quantification of the thickness of the pyramidal layer in (left) CA1 and (right) CA3. Scale bars: **B =** 1 mm, **C** = 500 µm

Figure S3: **CAR and adult neurogenesis**

A. Neurospheres were generated from NPCs isolated from the SGZ of 2 month-old WT mice. Representative immunoblots showing CAR and Sox-2 expression in

hippocampi, primary hippocampal neurons and neurospheres of adult NPCs from SGZ. **B**. 2-month-old mice were injected with thymidine analogues and brains were processed 28 days post-injection by IF. Confocal microscopy images showing cells positive for EdU and NeuN, and **C**. EdU and PSA-NCAM. Scale bar =10 µm

Figure S4: **Synaptic activity recruits CAR**.

A. Scheme of the mouse hippocampus illustrating electrodes placement to trigger LTP and record neuronal response. **B.** Representative immunofluorescence of hippocampal neurons with KCl treatment. Hippocampal neurons (DIV21) were treated with 5 mM KCl or 90 mM KCl for 5 min, fixed and stained for endogenous CAR and synaptophysin. Scale bars = 10 µm

Figure S5 : **The mobility of mice was examined using an open-field procedure**. Mice were placed in the center of an open box made in white Plexiglas equipped with infrared light-emitting diodes (50 x 50 cm, 50 cm high) and monitoring its movements for 10 min using Videotrack software (Viewpoint). (left) Locomotion activity was evaluated in terms of distance travelled (cm) and (right) locomotion speed calculated as total distance over time in movement (cm/s). The loss of CAR in the CNS did not alter locomotor behaviour. Locomotion of CT and CAR-CNS^{KO} mice in the open field for 10 min. Measurement of the distance travelled (left) and the speed (right) in CT and CAR-CNS^{KO} mice.

Figure S6 : **Downregulation of CAR by pro-inflammatory cytokines**. Representative immunoblot of three independent experiments. Human neurons-derived from IPS cells were incubated with increasing concentrations of TNF-α and IFN-γ for 72 h. β-tubulin was used as a loading control.

Figure S7: **Systemic LPS injection and hippocampal CAR levels**.

A. Immunoblot of total hippocampus extract from WT mice injected with PBS or LPS were sacrificed 7 days postinjection. Anti-b-tubulin and CAR Abs were used on the same membrane. b-tubulin was used as a loading control. **B.** Quantification from **A.** **C.** Immunoblot of total hippocampus extract from WT mice (the same genetic background as 3xTgAD mice) injected with PBS or LPS ; Mice were sacrificed for 7 weeks postinjection. β-tubulin was used as a loading control. **D.** Quantification from **C.** Results are expressed as means ± SEM, and the number of samples is indicated within the columns. N.S : non-significative. **B & D** values are normalized to 1.

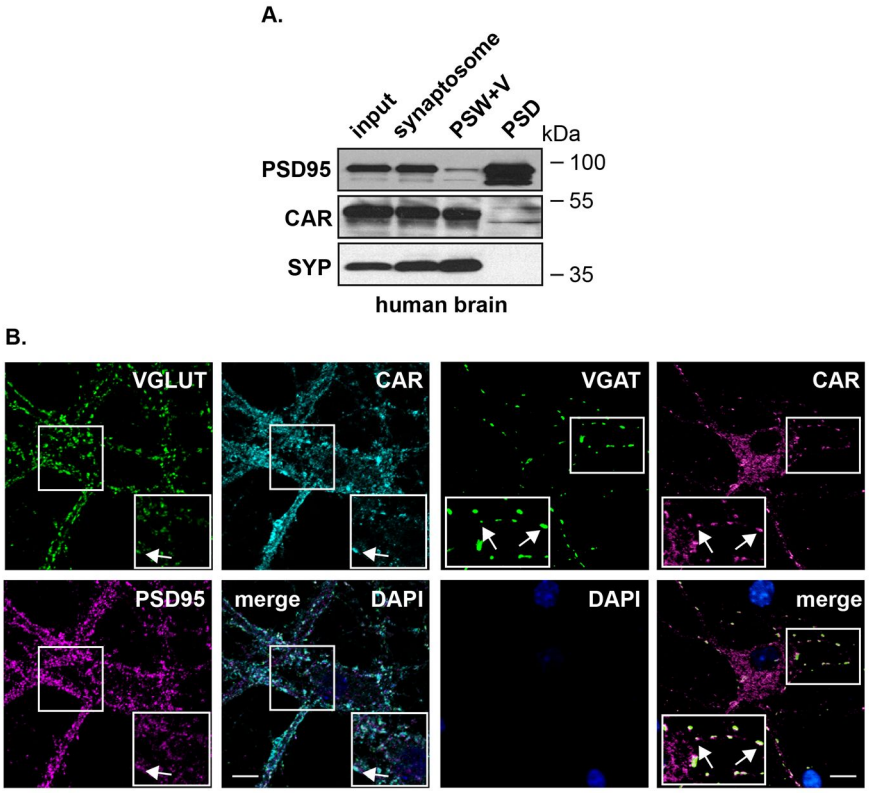
A.
input
synaptosome
PSW+V
PSD
kDa
PSD95
CAR
SYP
100
55
35
human brain
B.
VGLUT
CAR
VGAT
CAR
PSD95
merge
DAPI
DAPI
merge

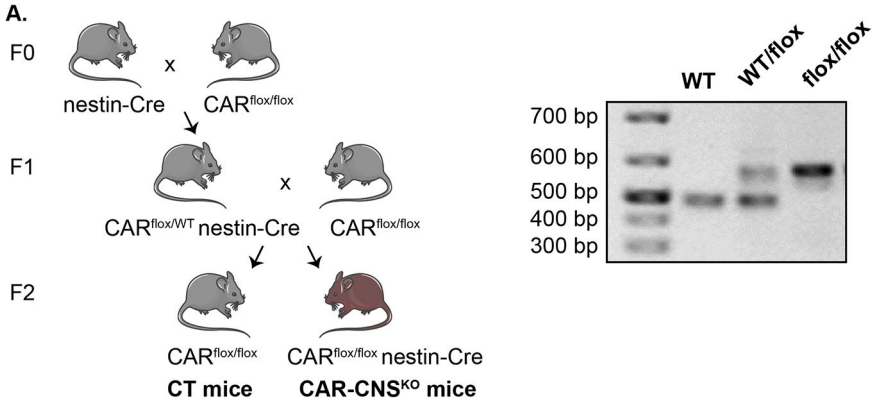
A.
F0
x
nestin-Cre
CAR flox/flox
F1
x
CAR flox/WT nestin-Cre
CAR flox/flox
F2
CAR flox/flox
CAR flox/flox nestin-Cre
CT mice
CAR-CNS KO mice
WT
WT/flox
flox/flox
700 bp
600 bp
500 bp
400 bp
300 bp

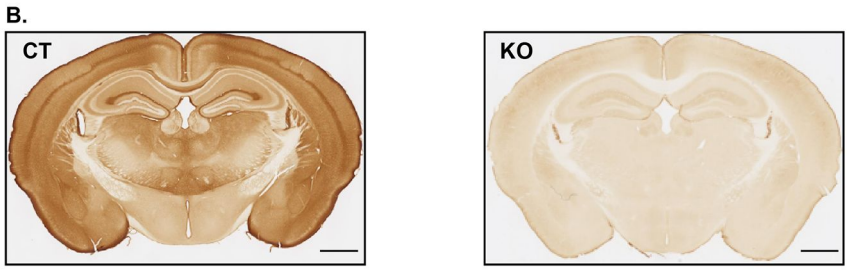
B.
CT
KO

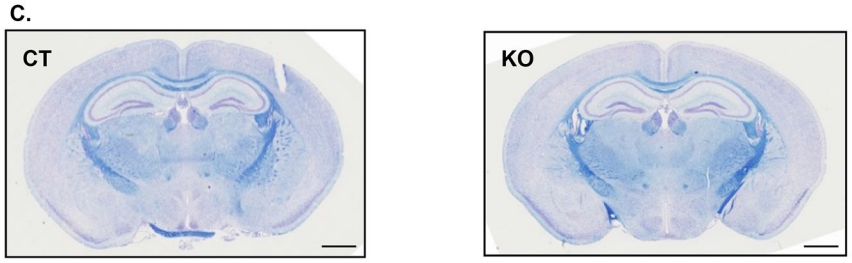
C.
CT
KO

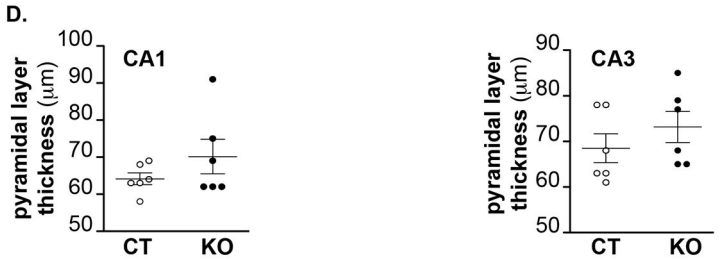
D.
CA1
pyramidal layer thickness (µm)
100
90
80
70
60
50
CT
KO
CA3
pyramidal layer thickness (µm)
90
80
70
60
50
CT
KO

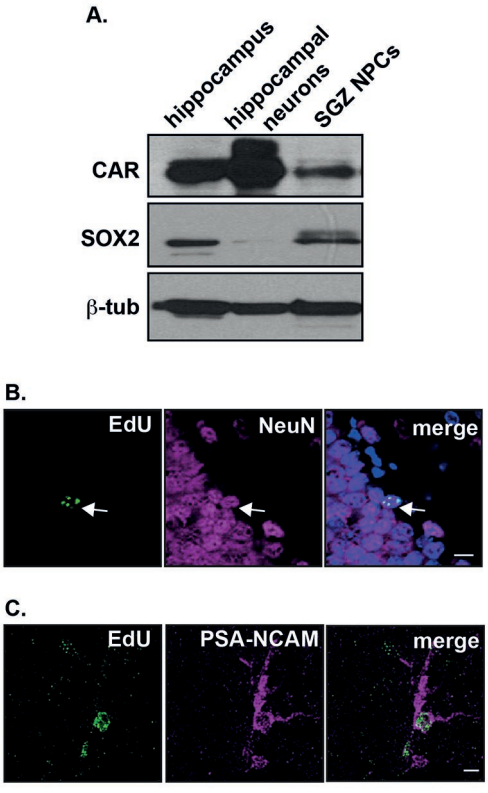
A.
hippocampus
hippocampal neurons
SGZ NPCs
CAR
SOX2
β-tub
B.
EdU
NeuN
merge
C.
EdU
PSA-NCAM
merge

A.

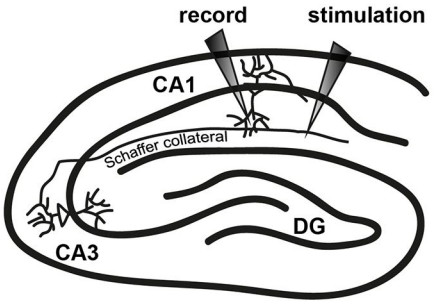
record
stimulation
CA1
Schaffer collateral
DG
CA3

B.

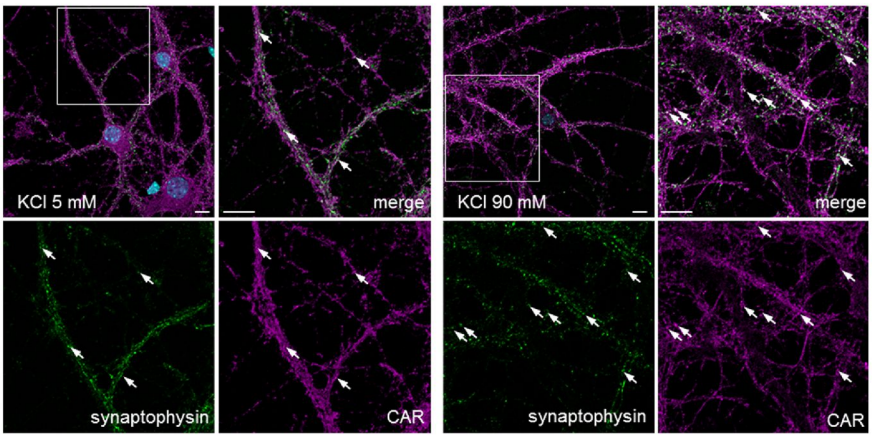
KCl 5 mM
merge
KCl 90 mM
merge
synaptophysin
CAR
synaptophysin
CAR

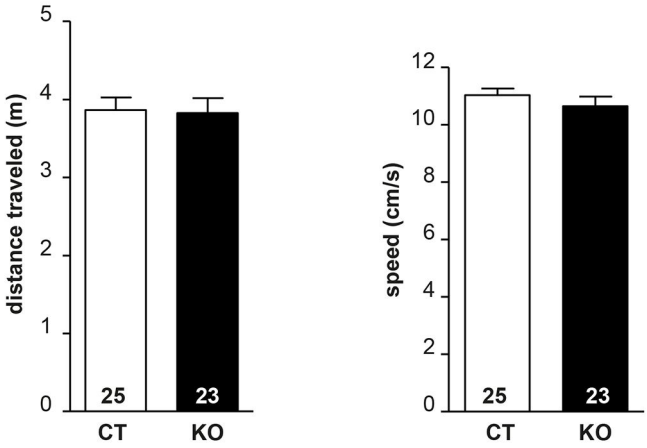
distance traveled (m)
5
4
3
2
1
0
25
23
CT
KO
speed (cm/s)
12
10
8
6
4
2
0
25
23
CT
KO

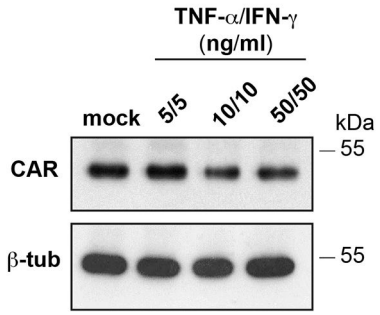
TNF-α/IFN-γ
(ng/ml)
mock
5/5
10/10
50/50
kDa
CAR
55
β-tub
55

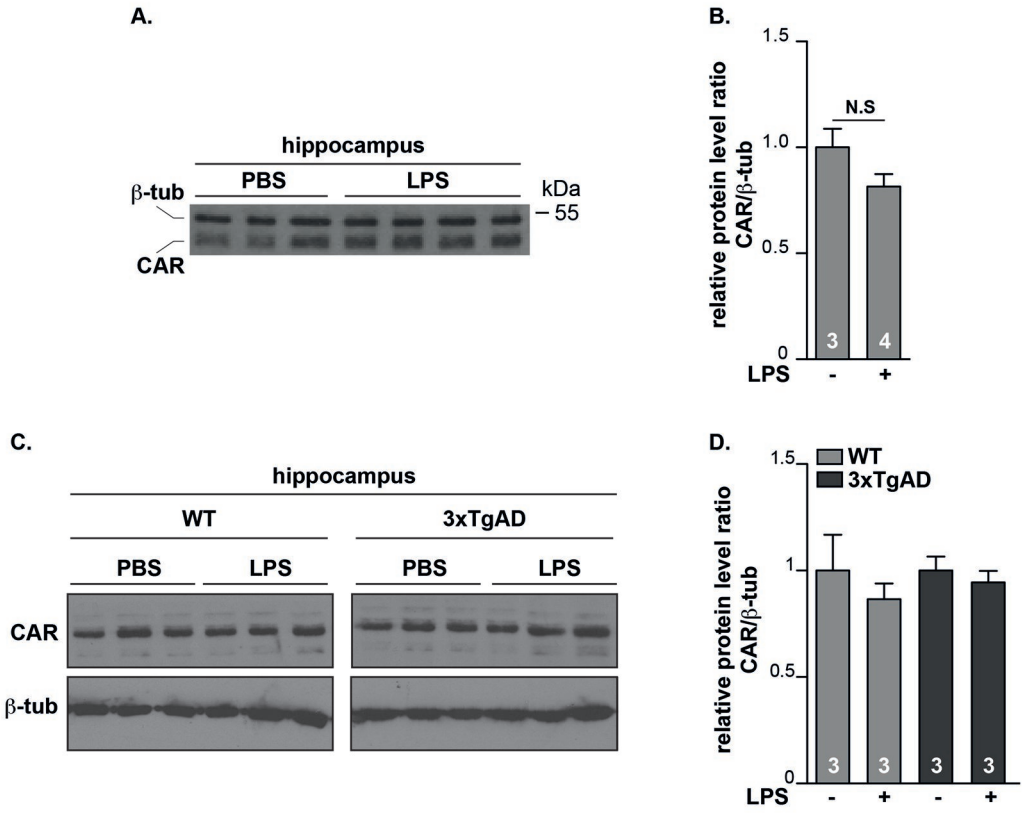
A.
hippocampus
PBS
LPS
β-tub
CAR
kDa
55
B.
relative protein level ratio
CAR/β-tub
1.5
1.0
0.5
0
N.S
3
4
LPS
-
+
C.
hippocampus
WT
3xTgAD
PBS
LPS
PBS
LPS
CAR
β-tub
D.
WT
3xTgAD
relative protein level ratio
CAR/β-tub
1.5
1
0.5
0
3
3
3
3
LPS
-
+
-
+